Memoirs of the Faculty of Engineering, Nagoya University
Vol 36, No. 2 (1984)

NUMERICAL ANALYSIS OF TRANSONIC FLOW AROUND A TWO-DIMENSIONAL AIRFOIL BY SOLVING FULL NAVIER-STOKES EQUATIONS

YI-YUN WANG and TOSHI FUJIWARA

Department of Aeronautical Engineering

(Received October 31, 1984)

Abstract

An effective finite-difference scheme for solving full compressible Navier-Stokes equations was initiated by Beam and Warming[1]. The purpose of this paper is to develop that technique and apply it to the calculations of several typical subsonic and transonic, inviscid and viscous steady flows for NACA 0012 airfoil.

Part of the analysis briefly contains the derivation process of all used formulas and the empirical treatments. Inviscid and viscous flows are analyzed separately, along with associated grid formation techniques and boundary conditions.

CONTENTS

1. Introduction

The Navier-Stokes equations, describing the flow of continuous fluid, were initiated more than one hundred years ago. However, it started being solved in a general sense only a few years ago. During last one century, generations of scientists made efforts in attempting to solve the equations. Prior to the appearance of a computer, they handled analytical solutions for a few typical problems using a series of approximations. Even in such problems, the mathematical knowledge used in the solution process has been very complicated. Hence, it has become well known that fluid mechanics is one of the hardest problems in physics. One had to depend mainly on experiments for practical applications.

The emergence of a computer provided the possibility of numerically solving the N-S equations. Due to the restrictions in computing speed and memory of early computers, one still had to give some approximate assumptions, and accordingly, the development of the CFD (Computational Fluid Dynamics) needed subsequent two stages; solving the potential and Euler equations. And then it entered the third stage, i. e., solving the N-S equations. In several advanced countries, the CFD has entered the fourth stage — investigating the cause and motion of vortices which are essentially unsteady problems and, of course, require a larger computer. But most countries are still making efforts to solve the N-S equations.

Because of the limitations in both computers and computational mathematics, the methods of solving the N-S equations had stayed on "solving boundary layer equations along with external inviscid ones" for a long time. To solve the N-S equations by treating the outflow (where convection is important) and the boundary layer (where the effects of viscosity balance with those of convections) simultaneously became possible only when super-computers appeared and finite-difference methods achieved rapid development during last decade. With respect to the theory of difference algorithms, the four developments stated below are important:

a) Unconditionally stable scheme[1~3]. Since rather small spatial steps must be adopted in the boundary layer, the computation time needed to have a convergent steady solution is found out to be about 3-6 times the one required for the disturbance to propagate from the body to the far boundary and to return back; this too lengthy calculation must be avoided by utilizing an unconditionally stable scheme.

b) Spatially factored[4~6]. The process advancing the solution forward is factored into the product of operators, each of which has only one spatial direction.

c) Delta-form[7]. Linearize all of the conservative flux vectors with respect to time. Then, $\Delta U^n = U^{n+1} - U^n$ become common unknown numbers.

d) Three-level scheme[1]. Implicitly center-differencing all viscous terms including cross derivatives will compose a set of difference equations containing 9 points which, however, are difficult to solve. Using the three-level scheme, cross derivative terms may be explicitly replaced by the values of previous time. Thus, the difference equations contain only 5 points (3 points in each direction); easy to solve.

The Beam-Warming scheme is equipped with the above four characteristics and as a result has been successfully applied to solving the full N-S equations, which had been a dream of numerous scientists in the field of fluid mechanics. The method is still popular in application to real CFD problems, although more modern and complicated modifications have been proposed.

In the present analysis, our calculations are limited to a simple contour — NACA 0012 airfoil, and to several typical subsonic and transonic as well as inviscid and viscous (lower Reynolds number) steady flows. The purpose of the research is to develop in more concrete forms the techniques stated in References 1 and 2. It is discovered that, for actual applications, there are many problems which need to be improved in the future.

2. Governing Equations

The two-dimensional compressible Navier-Stokes equations in Cartesian coordinates can be written in the conservation-law form

$$\frac{\partial U}{\partial t}+\frac{\partial F(U)}{\partial x}+\frac{\partial G(U)}{\partial y}=\frac{1}{Re}\left[\frac{\partial V_1(U,\ U_x)}{\partial x}\right.$$
$$\left.+\frac{\partial V_2(U,\ U_y)}{\partial x}+\frac{\partial W_1(U,\ U_x)}{\partial y}+\frac{\partial W_2(U,\ U_y)}{\partial y}\right], \tag{1}$$

where

$$U=\begin{pmatrix}\rho\\ \rho u\\ \rho v\\ e\end{pmatrix}=\begin{pmatrix}\rho\\ \bar{m}\\ \bar{n}\\ e\end{pmatrix},\qquad F(U)=\begin{pmatrix}\rho u\\ \rho u^2+p\\ \rho uv\\ (e+p)u\end{pmatrix}=\begin{pmatrix}\bar{m}\\ (\bar{m}^2/\rho)+p\\ \bar{m}\bar{n}/\rho\\ (e+p)\bar{m}/\rho\end{pmatrix},$$

$$G(U)=\begin{pmatrix}\rho v\\ \rho uv\\ \rho v^2+p\\ (e+p)v\end{pmatrix}=\begin{pmatrix}\bar{n}\\ \bar{m}\bar{n}/\rho\\ (\bar{n}^2/\rho)+p\\ (e+p)\bar{n}/\rho\end{pmatrix}, \tag{2}$$

$$V_1(U,\ U_x)=\begin{pmatrix}0\\ (\lambda+2\mu)u_x\\ \mu v_x\\ \mu vv_x+(\lambda+2\mu)uu_x+\kappa T_x\end{pmatrix},\qquad V_2(U,\ U_y)=\begin{pmatrix}0\\ \lambda v_y\\ \mu u_y\\ \mu vu_y+\lambda uv_y\end{pmatrix},$$

$$W_1(U,\ U_x)=\begin{pmatrix}0\\ \mu v_x\\ \lambda u_x\\ \mu uv_x+\lambda vu_x\end{pmatrix},\qquad W_2(U,\ U_y)=\begin{pmatrix}0\\ \mu u_y\\ (\lambda+2\mu)v_y\\ \mu uu_y+(\lambda+2\mu)vv_y+\kappa T_y\end{pmatrix},$$

$$p=(\gamma-1)\left(e-\frac{1}{2}\rho w^2\right) \qquad (\gamma=1.40),\ w^2=u^2+v^2, \tag{3}$$

$$T=\frac{p}{(\gamma-1)\rho}. \tag{4}$$

The variables ρ, u, v, p, e and T are the dimensionless density $\bar{\rho}/\bar{\rho}_\infty$, x-direction velocity component $\bar{u}/\bar{w}_\infty$, y-direction velocity component $\bar{v}/\bar{w}_\infty$, pressure $\bar{p}/(\bar{\rho}_\infty\bar{w}_\infty^2)$, total energy per unit volume $\bar{e}/(\bar{\rho}_\infty\bar{w}_\infty^2)$ and temperature $\bar{T}/(\bar{w}_\infty^2/C_v)$, respectively. The independent variables t, x and y are the dimensionless time $\bar{t}/(L/\bar{w}_\infty)$, coordinates $\bar{x}/L$ and $\bar{y}/L$, respectively. L is a reference length; usually the chord length of an airfoil is chosen as L. Finally, μ is the dimensionless viscosity coefficient $\bar{\mu}/\bar{\mu}_\infty$.

Using such a non-dimensional system, we easily obtain the freestream conditions: $\rho_\infty=1$, $u_\infty=\cos\alpha$, $v_\infty=\sin\alpha$, $p_\infty=1/(\gamma M_\infty^2)$, $e_\infty=p_\infty/(\gamma-1)+1/2$ and $T_\infty=p_\infty/(\gamma-1)$, where α is the angle of attack.

We adopt the Keyes semi-empirical formula[8] for the evaluation of $\bar{\mu}$, which can be applied to a wider temperature range while having a somewhat complex form;

$$\bar{\mu}=\frac{a_0\bar{T}^{3/2}}{\bar{T}+a\times10^b} \qquad \left(b=-\frac{a_1}{\bar{T}}\right), \tag{5}$$

where the constants for air are set to

$$a_0=1.488\times10^{-5},\ a=122.1,\ a_1=5 \quad (\bar{T}=79\sim1845\,K).$$

In the present calculation, $\bar{T}_\infty$ is assumed 288 K.

The dimensionless heat conductivity is shown as $\kappa=\gamma\mu/Pr$ (Prandtl number $Pr=0.75$), and λ is taken as $-(2/3)\mu$, the Stokes hypothesis.

3. Transformed Governing Equations

In order to change an irregular-shaped physical domain into a rectangular one, we have to introduce an appropriate transformation of independent variables. We are interested in those transformations independent of time because we only aim at the steady solution to the fundamental equations. In general, a transformation is expressed as

$$\xi=\xi(x,\ y),\ \eta=\eta(x,\ y),\ \tau=t. \tag{6}$$

The transformation Jacobian J is defined as

$$J=\xi_x\eta_y-\xi_y\eta_x=1/(x_\xi y_\eta-x_\eta y_\xi). \tag{7}$$

By solving the transformation identity

$$\begin{bmatrix}\xi_x & \xi_y\\ \eta_x & \eta_y\end{bmatrix}\begin{bmatrix}x_\xi & x_\eta\\ y_\xi & y_\eta\end{bmatrix}=\begin{bmatrix}1 & 0\\ 0 & 1\end{bmatrix},$$

we obtain

$$\xi_x = J y_\eta,\ \xi_y = -J x_\eta,\ \eta_x = -J y_\xi,\ \eta_y = J x_\xi. \tag{8}$$

Under such a transformation, the strong conservation-law form of the governing equations is still maintained[9], as shown in the following:

$$\begin{aligned}\frac{\partial U}{\partial t}+\frac{\partial D}{\partial x}+\frac{\partial E}{\partial y} &= \frac{\partial U}{\partial \tau}+\frac{\partial D}{\partial \xi}\xi_x+\frac{\partial D}{\partial \eta}\eta_x+\frac{\partial E}{\partial \xi}\xi_y+\frac{\partial E}{\partial \eta}\eta_y \\ &= \frac{\partial U}{\partial \tau}+J\left[\frac{\partial D}{\partial \xi}y_\eta-\frac{\partial D}{\partial \eta}y_\xi-\frac{\partial E}{\partial \xi}x_\eta+\frac{\partial E}{\partial \eta}x_\xi\right] \\ &= \frac{\partial U}{\partial \tau}+J\left[\frac{\partial (y_\eta D-x_\eta E)}{\partial \xi}+\frac{\partial(-y_\xi D+x_\xi E)}{\partial \eta}\right]=0.\end{aligned}$$

Define $\hat{U}=J^{-1}U$, $\hat{D}=y_\eta D-x_\eta E$ and $\hat{E}=-y_\xi D+x_\xi E$, and we have

$$\frac{\partial \hat{U}}{\partial \tau}+\frac{\partial \hat{D}}{\partial \xi}+\frac{\partial \hat{E}}{\partial \eta}=0.$$

Rewriting Eq. (1), we obtain the governing equations in the new coordinates as

$$\begin{aligned}&\frac{\partial \hat{U}}{\partial \tau}+\frac{\partial \hat{F}(U)}{\partial \xi}+\frac{\partial \hat{G}(U)}{\partial \eta} \\ &=\frac{1}{Re}\left[\frac{\partial \hat{V}_1(U,\ U_\xi)}{\partial \xi}+\frac{\partial \hat{V}_2(U,\ U_\eta)}{\partial \xi}+\frac{\partial \hat{W}_1(U,\ U_\xi)}{\partial \eta}+\frac{\partial \hat{W}_2(U,\ U_\eta)}{\partial \eta}\right],\end{aligned} \tag{9}$$

where

$$\begin{aligned}&\hat{U}=J^{-1}U, \\ &\hat{F}=y_\eta F-x_\eta G, \\ &\hat{G}=-y_\xi F+x_\xi G, \\ &V_1(U,\ U_x)+V_2(U,\ U_y)=J[y_\eta V_1(U,\ U_\xi)-y_\xi V_1(U,\ U_\eta) \\ &\qquad -x_\eta V_2(U,\ U_\xi)+x_\xi V_2(U,\ U_\eta)], \\ &W_1(U,\ U_x)+W_2(U,\ U_y)=J[y_\eta W_1(U,\ U_\xi)-y_\xi W_1(U,\ U_\eta) \\ &\qquad -x_\eta W_2(U,\ U_\xi)+x_\xi W_2(U,\ U_\eta)], \\ &\hat{V}_1(U,\ U_\xi)+\hat{V}_2(U,\ U_\eta)=y_\eta[V_1(U,\ U_x)+V_2(U,\ U_y)] \\ &\qquad -x_\eta[W_1(U,\ U_x)+W_2(U,\ U_y)], \\ &\hat{V}_1(U,\ U_\xi)=J[y_\eta^2 V_1(U,\ U_\xi)-x_\eta y_\eta V_2(U,\ U_\xi) \\ &\qquad -x_\eta y_\eta W_1(U,\ U_\xi)+x_\eta^2 W_2(U,\ U_\xi)], \\ &\hat{V}_2(U,\ U_\eta)=J[-y_\xi y_\eta V_1(U,\ U_\eta)+x_\xi y_\eta V_2(U,\ U_\eta) \\ &\qquad +x_\eta y_\xi W_1(U,\ U_\eta)-x_\xi x_\eta W_2(U,\ U_\eta)],\end{aligned} \tag{10}$$

$$\begin{aligned}\hat{W}_1(U,\ U_\xi)+\hat{W}_2(U,\ U_\eta)&=-y_\xi[V_1(U,\ U_x)+V_2(U,\ U_y)]\\&\quad+x_\xi[W_1(U,\ U_x)+W_2(U,\ U_y)],\\\hat{W}_1(U,\ U_\xi)&=J[-y_\xi y_\eta V_1(U,\ U_\xi)+x_\eta y_\xi V_2(U,\ U_\xi)\\&\quad+x_\xi y_\eta W_1(U,\ U_\xi)-x_\xi x_\eta W_2(U,\ U_\xi)],\\\hat{W}_2(U,\ U_\eta)&=J[y_\xi^2 V_1(U,\ U_\eta)-x_\xi y_\xi V_2(U,\ U_\eta)\\&\quad-x_\xi y_\xi W_1(U,\ U_\eta)+x_\xi^2 W_2(U,\ U_\eta)].\end{aligned}$$

In general, the body contour is transformed into a part of $\eta(x,\ y)=0$ if the transformation is of C-type. The remaining part is a specified cut in the flow field. Noting that there are relations between the velocities with respect to the two coordinate systems

$$\begin{bmatrix} d\xi/d\tau \\ d\eta/d\tau \end{bmatrix}=\begin{bmatrix} \hat{u} \\ \hat{v} \end{bmatrix}=J\begin{bmatrix} y_\eta & -x_\eta \\ -y_\xi & x_\xi \end{bmatrix}\begin{bmatrix} u \\ v \end{bmatrix},\ \begin{bmatrix} u \\ v \end{bmatrix}=\begin{bmatrix} x_\xi & x_\eta \\ y_\xi & y_\eta \end{bmatrix}\begin{bmatrix} \hat{u} \\ \hat{v} \end{bmatrix}, \qquad (11)$$

the impermeable condition over the body surface is embodied by $\hat{v}=0$.

Now we are going to derive a complementary relation, which will be used for the calculation of body surface points, i. e., the momentum equation in the direction normal to the body contour. It results in a simplified form by using $\hat{v}=0$.

Consider a vector $\vec{N}=(0,\ -y_\xi,\ x_\xi,\ 0)$, where the effective part $(-y_\xi,\ x_\xi)$ shows the normal direction of $\eta(x,\ y)=\text{const}$, and make a scalar product with Eq. (9). The left-hand side of a new momentum equation consists of the three terms:

(a) $$-y_\xi\frac{\partial(J^{-1}\rho u)}{\partial\tau}+x_\xi\frac{\partial(J^{-1}\rho v)}{\partial\tau}=\frac{\partial[J^{-1}\rho(-y_\xi u+x_\xi v)]}{\partial\tau}=\frac{\partial(J^{-2}\rho\hat{v})}{\partial\tau};$$

to use as a boundary condition of a steady flow, it is always set equal to 0.

(b) $$-y_\xi\frac{\partial[y_\eta(\rho u^2+p)-x_\eta(\rho uv)]}{\partial\xi}+x_\xi\frac{\partial[y_\eta(\rho uv)-x_\eta(\rho v^2+p)]}{\partial\xi}$$

$$=-y_\xi\frac{\partial(J^{-1}\rho u\hat{u}+y_\eta p)}{\partial\xi}+x_\xi\frac{\partial(J^{-1}\rho v\hat{u}-x_\eta p)}{\partial\xi}$$

$$=J^{-1}\hat{v}\frac{\partial(J^{-1}\rho\hat{u})}{\partial\xi}+J^{-1}\rho\hat{u}(-y_\xi u_\xi+x_\xi v_\xi)-(y_\xi y_\eta+x_\xi x_\eta)p_\xi$$

$$-(y_\xi y_{\xi\eta}+x_\xi x_{\xi\eta})p.$$

(c) $$-y_\xi\frac{\partial[-y_\xi(\rho u^2+p)+x_\xi(\rho uv)]}{\partial\eta}+x_\xi\frac{\partial[-y_\xi(\rho uv)+x_\xi(\rho v^2+p)]}{\partial\eta}$$

$$=-y_\xi\frac{\partial(J^{-1}\rho u\hat{v}-y_\xi p)}{\partial\eta}+x_\xi\frac{\partial(J^{-1}\rho v\hat{v}+x_\xi p)}{\partial\eta}$$

$$=J^{-1}\hat{v}\frac{\partial(J^{-1}\rho\hat{v})}{\partial\eta}+J^{-1}\rho\hat{v}(-y_{\xi}u_{\eta}+x_{\xi}v_{\eta})+(y_{\xi}{}^{2}+x_{\xi}{}^{2})p_{\eta}$$

$$+(y_{\xi}y_{\xi\eta}+x_{\xi}x_{\xi\eta})p.$$

Substituting the impermeable condition $\hat{v}=0$, we obtain

$$-(y_{\xi}y_{\eta}+x_{\xi}x_{\eta})p_{\xi}+(y_{\xi}{}^{2}+x_{\xi}{}^{2})p_{\eta}$$

$$=-J^{-1}\rho\hat{u}(-y_{\xi}u_{\xi}+x_{\xi}v_{\xi})+\vec{N}\cdot\frac{1}{Re}\left[\frac{\partial(\hat{V}_{1}+\hat{V}_{2})}{\partial\xi}+\frac{\partial(\hat{W}_{1}+\hat{W}_{2})}{\partial\eta}\right]. \qquad (12)$$

In the case of an inviscid flow, the second term of the right-hand side vanishes, whereas the first term vanishes for a viscous flow due to $\hat{u}=0$.

4. Difference Scheme

A single-step scheme for temporally advancing the solution of Eq. (9) was introduced by Beam and Warming[1], i. e.,

$$\varDelta\hat{U}^{n}=\frac{\theta\varDelta\tau}{1+\delta}\frac{\partial}{\partial\tau}\varDelta\hat{U}^{n}+\frac{\varDelta\tau}{1+\delta}\frac{\partial}{\partial\tau}\hat{U}^{n}+\frac{\delta}{1+\delta}\varDelta\hat{U}^{n-1}$$

$$+0\left[\left(\theta-\frac{1}{2}-\delta\right)\varDelta\tau^{2}+\varDelta\tau^{3}\right], \qquad (13)$$

where $\hat{U}^{n}=\hat{U}(n\varDelta\tau)$ and $\varDelta\hat{U}^{n}=\hat{U}^{n+1}-\hat{U}^{n}$. The parameters θ and δ may have various combinations, resulting in explicit or implicit, first-order- or second-order-accurate schemes. The schemes are implicit if $\theta>0$ and are three-level ones when $\delta>0$.

The accuracy of the algorithm (13) can be checked using simple manipulations as

$$(1+\delta)\left(\frac{\partial\hat{U}^{n}}{\partial\tau}\varDelta\tau+\frac{1}{2}\frac{\partial^{2}\hat{U}^{n}}{\partial\tau^{2}}\varDelta\tau^{2}\right)$$

$$\doteq\theta\varDelta\tau\left(\frac{\partial^{2}\hat{U}^{n}}{\partial\tau^{2}}\varDelta\tau\right)+\varDelta\tau\frac{\partial\hat{U}^{n}}{\partial\tau}-\delta\left(-\frac{\partial\hat{U}^{n}}{\partial\tau}\varDelta\tau+\frac{1}{2}\frac{\partial^{2}\hat{U}^{n}}{\partial\tau^{2}}\varDelta\tau^{2}\right),$$

$$\varDelta\tau\ :\ \ (1+\delta)\frac{\partial\hat{U}^{n}}{\partial\tau}-\frac{\partial\hat{U}^{n}}{\partial\tau}-\delta\frac{\partial\hat{U}^{n}}{\partial\tau}=0,$$

$$\varDelta\tau^{2}\ :\ \ \frac{1}{2}(1+\delta)\frac{\partial^{2}\hat{U}^{n}}{\partial\tau^{2}}-\theta\frac{\partial^{2}\hat{U}^{n}}{\partial\tau^{2}}+\frac{\delta}{2}\frac{\partial^{2}\hat{U}^{n}}{\partial\tau^{2}}=\left(\frac{1}{2}+\delta-\theta\right)\frac{\partial^{2}\hat{U}^{n}}{\partial\tau^{2}}.$$

With respect to the stability of the algorithm (13), Reference 1 listed only the conclusions for second-order-accurate algorithm ($\theta=\delta+1/2$): a) Applying it to a model linear scalar convection equation, it is unconditionally stable for $\delta>0$. b) Applying to a typical linear scalar diffusion equation, it is unconditionally stable for $\delta\geqslant0.385$. In the numerical examples shown later, we choose a combination $\theta=1$ and $\delta=1/2$. Obviously, it ensures second-order accuracy and is unconditionally stable which enables us to gradually increase the time increment.

Substituting Eq. (9) into Eq. (13), we obtain

$$
\begin{aligned}
\Delta\hat{U}^n=&\frac{\theta\Delta\tau}{1+\delta}\left[\frac{\partial}{\partial\xi}\left(-\Delta\hat{F}+\frac{\Delta\hat{V}_1+\Delta\hat{V}_2}{Re}\right)^n+\frac{\partial}{\partial\eta}\left(-\Delta\hat{G}+\frac{\Delta\hat{W}_1+\Delta\hat{W}_2}{Re}\right)^n\right]\\
&+\frac{\Delta\tau}{1+\delta}\left[\frac{\partial}{\partial\xi}\left(-\hat{F}+\frac{\hat{V}_1+\hat{V}_2}{Re}\right)^n+\frac{\partial}{\partial\eta}\left(-\hat{G}+\frac{\hat{W}_1+\hat{W}_2}{Re}\right)^n\right]\\
&+\frac{\delta}{1+\delta}\Delta\hat{U}^{n-1}+0\left[\left(\theta-\frac{1}{2}-\delta\right)\Delta\tau^2+\Delta\tau^3\right].
\end{aligned}
\tag{14}
$$

According to the Taylor series expansion

$$
\begin{aligned}
&\Delta\hat{F}^n=\left(\frac{\partial\hat{F}}{\partial\hat{U}}\right)^n\Delta\hat{U}^n+0(\Delta\tau^2)=\hat{A}^n\Delta\hat{U}^n+0(\Delta\tau^2),\\
&\Delta\hat{G}^n=\left(\frac{\partial\hat{G}}{\partial\hat{U}}\right)^n\Delta\hat{U}^n+0(\Delta\tau^2)=\hat{B}^n\Delta\hat{U}^n+0(\Delta\tau^2),\\
&\Delta\hat{V}_1{}^n=\left(\frac{\partial\hat{V}_1}{\partial\hat{U}}\right)^n\Delta\hat{U}^n+\left(\frac{\partial\hat{V}_1}{\partial\hat{U}_\xi}\right)^n\Delta\hat{U}_\xi{}^n+0(\Delta\tau^2)\\
&\qquad=\hat{P}^n\Delta\hat{U}^n+\hat{Q}^n\Delta\hat{U}_\xi{}^n+0(\Delta\tau^2)=(\hat{P}-\hat{Q}_\xi)^n\Delta\hat{U}^n+\frac{\partial}{\partial\xi}(\hat{Q}^n\Delta\hat{U}^n)+0(\Delta\tau^2),\\
&\Delta\hat{W}_2{}^n=\left(\frac{\partial\hat{W}_2}{\partial\hat{U}}\right)^n\Delta\hat{U}^n+\left(\frac{\partial\hat{W}_2}{\partial\hat{U}_\eta}\right)^n\Delta\hat{U}_\eta{}^n+0(\Delta\tau^2)\\
&\qquad=\hat{R}^n\Delta\hat{U}^n+\hat{S}^n\Delta\hat{U}_\eta{}^n+0(\Delta\tau^2)=(\hat{R}-\hat{S}_\eta)^n\Delta\hat{U}^n+\frac{\partial}{\partial\eta}(\hat{S}^n\Delta\hat{U}^n)+0(\Delta\tau^2),
\end{aligned}
\tag{15}
$$

where the notations $\hat{U}_\xi$ and $\hat{U}_\eta$ denote $J^{-1}U_\xi$ and $J^{-1}U_\eta$ and, in addition, we note Eq. (10) to obtain

$$
\begin{aligned}
&\hat{A}=\frac{\partial\hat{F}}{\partial\hat{U}}=\frac{\partial(y_\eta F-x_\eta G)}{J^{-1}\partial U}=J(y_\eta A-x_\eta B),\\
&\hat{B}=\frac{\partial\hat{G}}{\partial\hat{U}}=\frac{\partial(-y_\xi F+x_\xi G)}{J^{-1}\partial U}=J(-y_\xi A+x_\xi B),\\
&\hat{Q}=\frac{\partial\hat{V}_1}{\partial\hat{U}_\xi}=J^2\left[y_\eta{}^2\frac{\partial V_1(U,\ U_\xi)}{\partial U_\xi}-x_\eta y_\eta\frac{\partial V_2(U,\ U_\xi)}{\partial U_\xi}-x_\eta y_\eta\frac{\partial W_1(U,\ U_\xi)}{\partial U_\xi}\right.\\
&\qquad\left.+x_\eta{}^2\frac{\partial W_2(U,\ U_\xi)}{\partial U_\xi}\right]=J^2[y_\eta{}^2(QV)-x_\eta y_\eta(SV)-x_\eta y_\eta(QW)+x_\eta{}^2(SW)],\\
&\hat{S}=\frac{\partial\hat{W}_2}{\partial\hat{U}_\eta}=J^2\left[y_\xi{}^2\frac{\partial V_1(U,\ U_\eta)}{\partial U_\eta}-x_\xi y_\xi\frac{\partial V_2(U,\ U_\eta)}{\partial U_\eta}-x_\xi y_\xi\frac{\partial W_1(U,\ U_\eta)}{\partial U_\eta}\right.
\end{aligned}
\tag{16}
$$

$$+x_\xi{}^2\frac{\partial W_2(U,\ U_\eta)}{\partial U_\eta}\Bigg]=J^2[y_\xi{}^2(QV)-x_\xi y_\xi(SV)-x_\xi y_\xi(QW)+x_\xi{}^2(SW)].$$

The matrices A, B, QV, SV, QW and SW are derived in Appendix A. The matrices $\hat{P}-\hat{Q}_\xi$ and $\hat{R}-\hat{S}_\eta$ will be explained at the end of this section.

It is ingenious to let

$$\Delta\hat{V}_2{}^n=\Delta\hat{V}_2{}^{n-1}+0(\Delta\tau^2)\quad\text{and}\quad\Delta\hat{W}_1{}^n=\Delta\hat{W}_1{}^{n-1}+0(\Delta\tau^2). \tag{17}$$

Accordingly, the cross derivative viscous terms, which need four corner points and cause difficulty in implicitly solving difference equations, are conveniently replaced explicitly by the values of previous time without altering the accuracy of the scheme. Such treatment is very important for the full Navier-Stokes equations to be solved. Although we must handle a larger memory size by having one more level variables compared with the two-level scheme, this is rather trivial in comparison with the entire memory in use.

Substituting Eqs. (15), (16) and (17) into Eq. (14), we have

$$\begin{aligned}&\left\{I+\frac{\theta\Delta\tau}{1+\delta}\left[\frac{\partial}{\partial\xi}\left(\hat{A}-\frac{\hat{P}-\hat{Q}_\xi}{Re}\right)^n-\frac{1}{Re}\frac{\partial^2}{\partial\xi^2}\hat{Q}^n\right]+\frac{\theta\Delta\tau}{1+\delta}\left[\frac{\partial}{\partial\eta}\left(\hat{B}-\frac{\hat{R}-\hat{S}_\eta}{Re}\right)^n\right.\right.\\&\left.\left.-\frac{1}{Re}\frac{\partial^2}{\partial\eta^2}\hat{S}^n\right]\right\}\Delta\hat{U}^n=sign\,\delta\cdot\frac{\theta\Delta\tau}{1+\delta}\frac{1}{Re}\left[\frac{\partial}{\partial\xi}(\Delta\hat{V}_2{}^{n-1})+\frac{\partial}{\partial\eta}(\Delta\hat{W}_1{}^{n-1})\right]\\&+\frac{\Delta\tau}{1+\delta}\left[\frac{\partial}{\partial\xi}\left(-\hat{F}+\frac{\hat{V}_1+\hat{V}_2}{Re}\right)^n+\frac{\partial}{\partial\eta}\left(-\hat{G}+\frac{\hat{W}_1+\hat{W}_2}{Re}\right)^n\right]+\frac{\delta}{1+\delta}\Delta\hat{U}^{n-1}\\&+0\left[\left(\theta-\frac{1}{2}-\delta\right)\Delta\tau^2+\Delta\tau^3\right],\end{aligned} \tag{18}$$

where $sign\,\delta=1$ or 0, according to $\delta>0$ or $\delta=0$. In addition, the notation of the form

$$\left[\frac{\partial}{\partial\xi}\left(\hat{A}-\frac{\hat{P}-\hat{Q}_\xi}{Re}\right)^n\right]\Delta\hat{U}^n$$

signifies in reality

$$\frac{\partial}{\partial\xi}\left[\left(\hat{A}-\frac{\hat{P}-\hat{Q}_\xi}{Re}\right)^n\Delta\hat{U}^n\right],$$

throughout this paper. We then spatially factorize the left-hand side of Eq. (18) as follows:

$$\begin{aligned}&\left\{I+\frac{\theta\Delta\tau}{1+\delta}\left[\frac{\partial}{\partial\xi}\left(\hat{A}-\frac{\hat{P}-\hat{Q}_\xi}{Re}\right)^n-\frac{1}{Re}\frac{\partial^2}{\partial\xi^2}\hat{Q}^n\right]\right\}\\&\left\{I+\frac{\theta\Delta\tau}{1+\delta}\left[\frac{\partial}{\partial\eta}\left(\hat{B}-\frac{\hat{R}-\hat{S}_\eta}{Re}\right)^n-\frac{1}{Re}\frac{\partial^2}{\partial\eta^2}\hat{S}^n\right]\right\}\Delta\hat{U}^n=RHS\text{ of (18)}.\end{aligned} \tag{19}$$

As the spatial factorization causes only the error of $O(\Delta\tau^3)$, the temporal accuracy of Eq. (18) is not altered.

Before closing this section, it may be useful to present the derivation and explanation of $\hat{P}-\hat{Q}_\xi$ and $\hat{R}-\hat{S}_\eta$. From Eqs. (15) and (10), we have

$$\hat{P}=\frac{\partial \hat{V}_1}{\partial \hat{U}}=J^2\Big[y_\eta{}^2\frac{\partial V_1(U,\ U_\xi)}{\partial U}-x_\eta y_\eta\frac{\partial V_2(U,\ U_\xi)}{\partial U}$$

$$-x_\eta y_\eta\frac{\partial W_1(U,\ U_\xi)}{\partial U}+x_\eta{}^2\frac{\partial W_2(U,\ U_\xi)}{\partial U}\Big]$$

$$=J^2[y_\eta{}^2(PV\xi)-x_\eta y_\eta(RV\xi)-x_\eta y_\eta(PW\xi)+x_\eta{}^2(RW\xi)],$$

$$\hat{R}=\frac{\partial \hat{W}_2}{\partial \hat{U}}=J^2\Big[y_\xi{}^2\frac{\partial V_1(U,\ U_\eta)}{\partial U}-x_\xi y_\xi\frac{\partial V_2(U,\ U_\eta)}{\partial U}$$

$$-x_\xi y_\xi\frac{\partial W_1(U,\ U_\eta)}{\partial U}+x_\xi{}^2\frac{\partial W_2(U,\ U_\eta)}{\partial U}\Big]$$

$$=J^2[y_\xi{}^2(PV\eta)-x_\xi y_\xi(RV\eta)-x_\xi y_\xi(PW\eta)+x_\xi{}^2(RW\eta)],$$

where the matrices $PV\xi$ and $PV\eta$ are the matrix PVX in Appendix A, where the differential subscript x should be changed to ξ or η. Similarly, $RV\xi$ and $RV\eta$ are RVY, $PW\xi$ and $PW\eta$ are PWX, and $RW\xi$ and $RW\eta$ are RWY. Then, we obtain

$$\hat{P}-\hat{Q}_\xi=J^2\{y_\eta{}^2[(PV\xi)-(QV)_\xi]-x_\eta y_\eta[(RV\xi)-(SV)_\xi]$$

$$-x_\eta y_\eta[(PW\xi)-(QW)_\xi]+x_\eta{}^2[(RW\xi)-(SW)_\xi]\},$$

$$\hat{R}-\hat{S}_\eta=J^2\{y_\xi{}^2[(PV\eta)-(QV)_\eta]-x_\xi y_\xi[(RV\eta)-(SV)_\eta] \tag{20}$$

$$-x_\xi y_\xi[(PW\eta)-(QW)_\eta]+x_\xi{}^2[(RW\eta)-(SW)_\eta]\}.$$

Analogously the matrices $(PV\xi)-(QV)_\xi$ and $(PV\eta)-(QV)_\eta$ correspond to $(PVX)-(QV)_x$ in Appendix A. $(RV\xi)-(SV)_\xi$ and $(RV\eta)-(SV)_\eta$ to $(RVY)-(SV)_y$, $(PW\xi)-(QW)_\xi$ and $(PW\eta)-(QW)_\eta$ to $(PWX)-(QW)_x$, and $(RW\xi)-(SW)_\xi$ and $(RW\eta)-(SW)_\eta$ to $(RWY)-(SW)_y$.

Thus we can easily find $\hat{P}-\hat{Q}_\xi=\hat{\alpha}\mu_T+\hat{\beta}\mu_\xi$ and $\hat{R}-\hat{S}_\eta=\hat{\gamma}\mu_T+\hat{\delta}\mu_\eta$, where

$$\mu_T=\frac{d\mu}{dT}=\frac{d(\bar{\mu}/\bar{\mu}_\infty)}{d(\bar{T}\cdot T_\infty/\bar{T}_\infty)}=\frac{1}{\bar{\mu}_\infty}\frac{d\bar{\mu}}{d\bar{T}}\frac{\bar{T}_\infty}{T_\infty}$$

$$=\mu\Big[\frac{d\bar{\mu}}{\bar{\mu}d\bar{T}}\Big]\frac{\bar{T}_\infty}{T_\infty}=\mu\Big[\frac{d(\log\bar{\mu})}{d\bar{T}}\Big]\frac{\bar{T}_\infty}{T_\infty}. \tag{21}$$

Applying the Keyes formula (5), we obtain

$$\frac{d(\log\bar{\mu})}{d\bar{T}}=\frac{3}{2}\frac{1}{\bar{T}}-\frac{1+a\cdot a_1\cdot\log 10\cdot\exp(-a_1\cdot\log 10/\bar{T})/\bar{T}^2}{\bar{T}+a\cdot\exp(-a_1\cdot\log 10/\bar{T})}. \tag{22}$$

In subsonic or transonic regions, there are not strong shock waves, yielding the temperature gradient rather small. Therefore, $\hat{P}-\hat{Q}_\xi$ and $\hat{R}-\hat{S}_\eta$ may be neglected.

5. Addition of Dissipative Terms

The practical process of numerically solving a system, consisting of difference equations and boundary conditions, is always accompanied by the propagation of errors which satisfy the same difference equations and the boundary conditions imposing "exactly equal to zero". If the propagation of errors can be controlled within a certain limit, the numerical solution of that system can still be regarded as an approximation of the exact solution; this is called "stable". One of the methods analyzing the stability of difference equations is the von Neumann method. Assume that $g^n(k)e^{Iik\Delta x}$ is a Fourier component corresponding to the wave number k at the point $(n\Delta t,\ i\Delta x)$, while at the next time step the component becomes $g^{n+1}(k)e^{Iik\Delta x}$. Then, the amplification factor $G(k)$ is defined as follows:

$$G(k)=g^{n+1}(k)/g^n(k)=|G(k)|e^{I\varphi}.$$

Here the criterion $|G(k)|<1$ or $|G(k)|>1$ is used to judge whether the error is attenuated or amplified. $\varphi>0$ or $\varphi<0$ corresponds to whether the phase is ahead or behind, a phenomenon called dispersion. Although large dispersion is not desirable a far more important condition is $|G(k)|<1$. The existence of only a few wave numbers k which yield $|G(k)|=1$ may be permitted. Because of dispersion, the error may practice damping at the next time step even if it has not caused attenuation at the present time step. Note, however, that the existence of these wave numbers always slows down the process of convergence. In general, therefore, one artificially adds high-order dissipative terms to accelerate the attenuation. A simple method is to append to the right-hand side of algorithm (13) the fourth-order dissipative term

$$\Omega J^{-1}[(\nabla_\xi\Delta_\xi)^2+(\nabla_\eta\Delta_\eta)^2]J\hat{U}^n, \tag{23}$$

where ∇ and Δ are the conventional notations of backward and forward differences, rendering $\nabla_\xi\Delta_\xi U_{i,\,j}=U_{i+1,\,j}-2U_{i,\,j}+U_{i-1,\,j}$, $(\nabla_\xi\Delta_\xi)^2U_{i,\,j}=U_{i+2,\,j}-4U_{i+1,\,j}+6U_{i,\,j}-4U_{i-1,\,j}+U_{i-2,\,j}$, etc.. Note that the dissipative term has been multiplied by a Jacobian determinant and divided by the same one outside, to maintain a freestream solution; therefore, the dissipative term is not conservationally differenced.

Assuming that $\Delta\tau$ is sufficiently small, let us examine the stability of algorithm (13) after adding the dissipative term (23) to one-dimensional equation:

$$\Delta u^n=\frac{\delta}{1+\delta}\Delta u^{n-1}-\Omega(\nabla_x\Delta_x)^2u^n,$$

$$G-1=\frac{\delta}{1+\delta}\left(1-\frac{1}{G}\right)-\Omega(e^{2Ik\Delta x}-4e^{Ik\Delta x}+6-4e^{-Ik\Delta x}+e^{-2Ik\Delta x}),$$

$$G(G-1)=\frac{\delta}{1+\delta}(G-1)-\Omega G\cdot4(1-\cos k\Delta x)^2,$$

$$G^2-\left[1+\frac{\delta}{1+\delta}-4\Omega(1-\cos k\Delta x)^2\right]G+\frac{\delta}{1+\delta}=0.$$

G has two real roots 1 and $\delta/(1+\delta)$ if $\Omega=0$. When increasing Ω from zero, the following situations appear in turn: a) Two same real roots $[\delta/(1+\delta)]^{1/2}$. b) A pair of complex conjugate roots with their moduli $[\delta/(1+\delta)]^{1/2}$. c) Two same real roots $-[\delta/(1+\delta)]^{1/2}$. d) Two real roots -1 and $-\delta/(1+\delta)$. e) The modulus of one of the two roots will exceed 1, if continuously increasing Ω. Thus, the stability condition is written as

$$0\leqslant 4\Omega(1-\cos k\Delta x)^2\leqslant 16\Omega\leqslant 2\left(1+\frac{\delta}{1+\delta}\right),$$

which can be rewritten as

$$0\leqslant\Omega\leqslant\frac{1+2\delta}{8(1+\delta)}. \tag{24}$$

Steger[2)] suggested to implicitly add a second-order dissipative term on the left-hand side of algorithm (13), which tends to zero when the solution converges to a steady one. However, the stability bound (24) is widened twice, as shown below. Accordingly, we can use larger dissipative terms to accelerate the converging process. We slightly modify the above verification:

$$\Delta u^n-\Omega\nabla_x\Delta_x(\Delta u^n)=\frac{\delta}{1+\delta}\Delta u^{n-1}-\Omega(\nabla_x\Delta_x)^2u^n,$$

$$(G-1)[1+2\Omega(1-\cos k\Delta x)]=\frac{\delta}{1+\delta}\frac{G-1}{G}-4\Omega(1-\cos k\Delta x)^2,$$

$$G^2-\left[1+\frac{1}{1+2\Omega(1-\cos k\Delta x)}\frac{\delta}{1+\delta}-\frac{4\Omega(1-\cos k\Delta x)^2}{1+2\Omega(1-\cos k\Delta x)}\right]G$$

$$+\frac{1}{1+2\Omega(1-\cos k\Delta x)}\frac{\delta}{1+\delta}=0. \tag{25}$$

Thus, the stability condition is

$$0\leqslant\frac{4\Omega(1-\cos k\Delta x)^2}{1+2\Omega(1-\cos k\Delta x)}\leqslant 2\left[1+\frac{1}{1+2\Omega(1-\cos k\Delta x)}\frac{\delta}{1+\delta}\right],$$

$$0\leqslant\Omega[(1-\cos k\Delta x)^2-(1-\cos k\Delta x)]\leqslant 2\Omega\leqslant\frac{1}{2}\left(1+\frac{\delta}{1+\delta}\right),$$

which reduces to

$$0\leqslant\Omega\leqslant\frac{1+2\delta}{4(1+\delta)}. \tag{26}$$

It is difficult to construct a fourth-order dissipative term at points adjacent to the boundary surfaces. In such cases, we replace $-\Omega J^{-1}(\nabla_\sigma\Delta_\sigma)^2U^n$ (σ is ξ or η) by $+\Omega J^{-1}(\nabla_\sigma\Delta_\sigma)U^n$ (note the sign). Then, Eq. (25) becomes

$$G^2-\left[1+\frac{1}{1+2\Omega(1-\cos k\Delta x)}\frac{\delta}{1+\delta}-\frac{2\Omega(1-\cos k\Delta x)}{1+2\Omega(1-\cos k\Delta x)}\right]G$$

$$+\frac{1}{1+2\Omega(1-\cos k\Delta x)}\frac{\delta}{1+\delta}=0,$$

the stability condition of which is the inequality

$$0 \leqslant \frac{2\Omega(1-\cos k\Delta x)}{1+2\Omega(1-\cos k\Delta x)} \leqslant 2\left[1+\frac{1}{1+2\Omega(1-\cos k\Delta x)}\frac{\delta}{1+\delta}\right].$$

This condition is automatically satisfied for all positive Ω; in other words, such a scheme is unconditionally stable.

Finally, it may be convenient if we explicitly write down the computational formulas, which is derived by adding the dissipative terms to Eq. (18) :

$$RHS = sign\,\delta\cdot\frac{\theta\Delta\tau}{1+\delta}\frac{1}{Re}\left[\frac{\partial}{\partial\xi}(\Delta\hat{V}_2{}^{n-1})+\frac{\partial}{\partial\eta}(\Delta\hat{W}_1{}^{n-1})\right]$$
$$+\frac{\Delta\tau}{1+\delta}\left[\frac{\partial}{\partial\xi}\left(-\hat{F}+\frac{\hat{V}_1+\hat{V}_2}{Re}\right)^n+\frac{\partial}{\partial\eta}\left(-\hat{G}+\frac{\hat{W}_1+\hat{W}_2}{Re}\right)^n\right]$$
$$+\frac{\delta}{1+\delta}\Delta\hat{U}^{n-1}-\Omega J^{-1}[(\nabla_\xi\Delta_\xi)^2+(\nabla_\eta\Delta_\eta)^2]J\hat{U}^n, \qquad (27)$$

$$\left\{I+\frac{\theta\Delta\tau}{1+\delta}\left[\frac{\partial}{\partial\xi}\left(\hat{A}-\frac{\hat{P}-\hat{Q}_\xi}{Re}\right)^n-\frac{1}{Re}\frac{\partial^2}{\partial\xi^2}\hat{Q}^n\right]-\Omega J^{-1}\nabla_\xi\Delta_\xi J\right\}\Delta\hat{U}^* = RHS, \qquad (28)$$

$$\left\{I+\frac{\theta\Delta\tau}{1+\delta}\left[\frac{\partial}{\partial\eta}\left(\hat{B}-\frac{\hat{R}-\hat{S}_\eta}{Re}\right)^n-\frac{1}{Re}\frac{\partial^2}{\partial\eta^2}\hat{S}^n\right]-\Omega J^{-1}\nabla_\eta\Delta_\eta J\right\}\Delta\hat{U}^n = \Delta\hat{U}^*, \qquad (29)$$

$$U^{n+1} = U^n + J\Delta\hat{U}^n. \qquad (30)$$

Because the solution procedures are gone through separately in ξ and η directions, the stability condition (26) obtained for one-dimensional equations is still effective. In general, it is adequate to place the coefficient Ω right at the center of both stability bounds, thereby establishing that the dissipation is effective and yet safe.

6. Method of Solving Block-Tridiagonal Equations

Eqs. (28) and (29) give two sets of equations of block-tridiagonal form. The method of solution is similar of that for scalar tridiagonal equations, which essentially is a kind of elimination method.

Consider a set of equations

$$\begin{bmatrix} b_1 & c_1 & & & & \\ a_2 & b_2 & c_2 & & & \\ & & \cdots & & & \\ & & a_l & b_l & c_l & \\ & & & & \cdots & \\ & & & & a_m & b_m \end{bmatrix}\begin{bmatrix} u_1 \\ u_2 \\ \cdots \\ u_l \\ \cdots \\ u_m \end{bmatrix} = \begin{bmatrix} d_1 \\ d_2 \\ \cdots \\ d_l \\ \cdots \\ d_m \end{bmatrix} \qquad (31)$$

By using elimination procedure in turn, it is converted into

$$\begin{bmatrix} 1 & c_1' & & & & \\ & 1 & c_2' & & & \\ & & \cdots & & & \\ & & & 1 & c_l' & \\ & & & & \cdots & \\ & & & & & 1 \end{bmatrix} \begin{bmatrix} u_1 \\ u_2 \\ \cdots \\ u_l \\ \cdots \\ u_m \end{bmatrix} = \begin{bmatrix} d_1' \\ d_2' \\ \cdots \\ d_l' \\ \cdots \\ d_m' \end{bmatrix} \tag{32}$$

where

$$c_l' = c_l \cdot (b_l - a_l c_{l-1}')^{-1}, \quad d_l' = (d_l - a_l d_{l-1}')(b_l - a_l c_{l-1}')^{-1} \quad (l=1, 2, \cdots, m). \tag{33}$$

$a_1=0$ and $c_m=0$ are obvious from Eq. (31). It is essential to find that Eq. (32) directly provides $u_m=d'_m$. Then we can explicitly solve the other u_l from u_m:

$$u_l = d'_l - c'_l u_{l+1} \quad (l=m-1, m-2, \cdots, 1). \tag{34}$$

When centered differences are used, Eqs. (28) and (29) result in the form identical to Eq. (31), where the notations a_l, b_l and c_l are 4×4 matrices and u_l and d_l are 4×1 matrices; thus they are called block-tridiagonal equations. Naturally, the results (33) and (34) can also be applied. Note that $(b_l - a_l c'_{l-1})^{-1}$ in Eq. (33) is the inversion of the matrix. From the viewpoint of saving the computing time of matrix inversion, it is adequate to program an inversion subroutine by ourselves. Assume $P=(p_{i,j})$ and $Q=P^{-1}=(q_{i,j})$. Hence,

$$q_{i,j} = \frac{(-1)^{i+j}}{|P|} \overline{P}_{j,i}, \tag{35}$$

where $|P|$ denotes the determinant of a matrix P and $\overline{P}_{j,i}$ denotes a cofactor determinant of P; for example, we have

$$\overline{P}_{3,2} = \begin{vmatrix} p_{11} & p_{13} & p_{14} \\ p_{21} & p_{23} & p_{24} \\ p_{41} & p_{43} & p_{44} \end{vmatrix}, \tag{36}$$

which gives

$$|P| = \sum_{j=1}^{4} p_{1,j} (-1)^{1+j} \overline{P}_{1,j}. \tag{37}$$

7. Grid Generation

A common difficulty which annoys finite difference practitioners is the irregularity of a physical domain. It not only makes the grid points adjacent to boundaries irregular and leads to frequent use of interpolation and extrapolation in constructing difference equations at those points, but also severely drops the accuracy of boundary conditions. Accordingly, such a mathematical transformation is desirable, that transforms the irregular physical domain to a rectangular computational one, where, naturally, the boundaries are transformed into straight lines parallel with the coordinate axes.

The advantages of using such a body-conforming transformation are[9]: a) A grid system of identical interval can be adopted in a rectangular computational domain. Consequently, the accuracy of difference at points adjacent to boundaries can be identical with that of other interior points. b) The boundary conditions can be accurately imposed. c) To improve accuracy, curvilinear grids may be clustered in the domain where the flow variables have large gradients. d) Equal treatment of the points adjacent to boundaries will be helpful to effectively use a vector-processing computer.

The transformations that one frequently uses, briefly speaking, basically consist of the following three types:

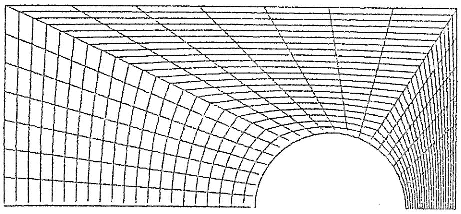

Figure 1
The curvilinear co-ordinate system generated by the following parametrization:

$$\vec{F}(0,\ t)=\begin{bmatrix}-2.5t+.5\\-2\end{bmatrix},\ \vec{F}(1,\ t)=\begin{bmatrix}0.5t+2\\-2\end{bmatrix}$$

$$\vec{F}(s,\ 0)=\begin{bmatrix}1.25-.75\cos(\pi s)\\-2+.75\sin(\pi s)\end{bmatrix}$$

$$\vec{F}(s,\ 1)=\begin{pmatrix}\begin{cases}-2, & 0.0\leq s<.33\\-6.5+13.5s, & .33\leq s<.66\\2.5, & .66\leq s\leq 1\end{cases}\\ \begin{cases}-2+6s, & 0.0\leq s<.33\\0.0, & .33\leq s<.66\\4-6s, & .66\leq s\leq 1\end{cases}\end{pmatrix}.$$

a) Algebraic construction. Fig. 1 is an example[10]. Its characteristics is simplicity in general; The method may be written into a formula only including elementary functions and therefore may have negligible computing time. Moreover, it is easy to cluster in specific domains and as a result it is usually adopted as a basis of adaptive grids. One of its faults is non-orthogonality, which causes large error. Another is non-analyticity. There are lines (or surfaces) within a domain where the first-order differential is discontinuous if boundaries include such points (or lines). Mathematically speaking, the transformation is not exact.

b) Conformal mapping[11]. This is an older technique. It is orthogonal and analytical within the domain. But it is rather difficult to find such a mapping for a general two-dimensional domain and is almost impossible for that of three-dimension. Therefore, those who prefer using this technique are still few although it has some developments recently.

c) Grid generation using elliptic-type differential equations[12~14]. A recent idea is to find a numerical solution of a system of partial differential equations and regard it as a transformation, the concrete form of which is not required to know. If the corresponding points on the entire closed boundary of a domain are specified, then utilizing the theory of partial differential eouations, the first-kind boundary-value problem is correct only for elliptic-type equations, e.g., the Laplace or Poisson equations. For such transformations, one of the properties is monotony. The extremum principle of elliptic equations, i.e., that extremum of solutions can not occur within the domain, assures the monotony of solutions along either coordinate direction ξ or η from one boundary to another. In other words, such a trans formation gives strictly a one-to-one mapping between physical and transformed domains. Another property is analyticity. The boundary slope discontinuities do not propagate into the domain. Due to the above-mentioned advantages, the transformations of this type are widely used recently. However, due to non-orthogonality, the high skewness between a coordinate line and a boundary will drop the accuracy of boundary conditions. There are several attempts to improve it.

Consider a transformation

$$\xi=\xi(x,\ y),\quad \eta=\eta(x,\ y),$$

which satisfies the Poisson equations

$$\nabla^2\xi=P,\quad \nabla^2\eta=Q. \tag{38}$$

The grid system on the computational plane $(\xi,\ \eta)$ will be rectangular, so that we are interested in the inverse transformation $x=x(\xi,\ \eta)$, $y=y(\xi,\ \eta)$ where the equations they must satisfy are derived in the following. The relations of first-order differentials between two transformations are

$$\begin{aligned}
&\frac{\partial x}{\partial x}=x_\xi\xi_x+x_\eta\eta_x=1,\\
&\frac{\partial x}{\partial y}=x_\xi\xi_y+x_\eta\eta_y=0,\\
&\frac{\partial y}{\partial x}=y_\xi\xi_x+y_\eta\eta_x=0,\\
&\frac{\partial y}{\partial y}=y_\xi\xi_y+y_\eta\eta_y=1,
\end{aligned} \tag{39}$$

which provide

$$\xi_x=Jy_\eta,\ \ \xi_y=-Jx_\eta,\ \ \eta_x=-Jy_\xi,\ \ \eta_y=Jx_\xi$$

$$(J=\xi_x\eta_y-\xi_y\eta_x=(x_\xi y_\eta-x_\eta y_\xi)^{-1}). \tag{40}$$

Differentiating the former two relations of Eq. (39), we obtain

$$\frac{\partial^2 x}{\partial x^2}=x_{\xi\xi}(\xi_x)^2+x_{\xi\eta}\eta_x\xi_x+x_\xi\xi_{xx}+x_{\eta\xi}\xi_x\eta_x+x_{\eta\eta}(\eta_x)^2+x_\eta\eta_{xx}=0, \tag{41}$$

$$\frac{\partial^2 x}{\partial y^2}=x_{\xi\xi}(\xi_y)^2+x_{\xi\eta}\eta_y\xi_y+x_\xi\xi_{yy}+x_{\eta\xi}\xi_y\eta_y+x_{\eta\eta}(\eta_y)^2+x_\eta\eta_{yy}=0. \tag{42}$$

Adding them up and using Eqs. (38) and (40), we obtain the differential equation with regard to x,

$$\alpha x_{\xi\xi}-2\beta x_{\xi\eta}+\gamma x_{\eta\eta}=-J^{-2}(Px_\xi+Qx_\eta)=\varphi. \tag{43}$$

Likewise, by differentiating the latter two relations of Eq. (39), we obtain

$$\alpha y_{\xi\xi}-2\beta y_{\xi\eta}+\gamma y_{\eta\eta}=-J^{-2}(Py_\xi+Qy_\eta)=\psi, \tag{44}$$

where

$$\alpha=x_\eta{}^2+y_\eta{}^2,\quad \beta=x_\xi x_\eta+y_\xi y_\eta,\quad \gamma=x_\xi{}^2+y_\xi{}^2. \tag{45}$$

In the solution process, α, β, γ, φ and ψ are evaluated as known numbers on n-level, whereas $x_{\xi\xi}$, $x_{\xi\eta}$, $x_{\eta\eta}$, etc. are centrally differenced using $n+1$-level unknown quantities; as a typical example, the difference form of Eq. (43) is

$$\begin{aligned}&C_{i,\,j}x^{(n+1)}_{i,\,j}+C_{i+1,\,j}x^{(n+1)}_{i+1,\,j}+C_{i+1,\,j+1}x^{(n+1)}_{i+1,\,j+1}+C_{i,\,j+1}x^{(n+1)}_{i,\,j+1}+C_{i-1,\,j+1}x^{(n+1)}_{i-1,\,j+1}\\&+C_{i-1,\,j}x^{(n+1)}_{i-1,\,j}+C_{i-1,\,j-1}x^{(n+1)}_{i-1,\,j-1}+C_{i,\,j-1}x^{(n+1)}_{i,\,j-1}+C_{i+1,\,j-1}x^{(n+1)}_{i+1,\,j-1}=\varphi_{i,\,j},\end{aligned} \tag{46}$$

where

$$\begin{aligned}&C_{i,\,j}=-2\left[\frac{\alpha}{(\Delta\xi)^2}+\frac{\gamma}{(\Delta\eta)^2}\right],\\&C_{i+1,\,j}=C_{i-1,\,j}=\frac{\alpha}{(\Delta\xi)^2},\\&C_{i,\,j+1}=C_{i,\,j-1}=\frac{\gamma}{(\Delta\eta)^2},\\&-C_{i+1,\,j+1}=C_{i-1,\,j+1}=-C_{i-1,\,j-1}=C_{i+1,\,j-1}=\frac{\beta}{2\Delta\xi\Delta\eta}.\end{aligned} \tag{47}$$

In solving Eq. (46), the ADI (Alternating Direction Implicit) method is a convenient procedure and particularly effective for a vector-processing computer. We found that SOR (Successive Over Relaxation) method is also fast in convergence on a scalar-processing computer FACOM M-382. Assume

$$\begin{aligned}r_{i,\,j}=&C_{i,\,j}x^{(n)}_{i,\,j}+C_{i+1,\,j}x^{(n)}_{i+1,\,j}+C_{i+1,\,j+1}x^{(n)}_{i+1,\,j+1}+C_{i,\,j+1}x^{(n)}_{i,\,j+1}+C_{i-1,\,j+1}x^{(n+1)}_{i-1,\,j+1}\\&+C_{i-1,\,j}x^{(n+1)}_{i-1,\,j}+C_{i-1,\,j-1}x^{(n+1)}_{i-1,\,j-1}+C_{i,\,j-1}x^{(n+1)}_{i,\,j-1}+C_{i+1,\,j-1}x^{(n)}_{i+1,\,j-1}-\varphi_{i,\,j},\end{aligned} \tag{48}$$

where the rule of determining superscript n or $n+1$ is to use the new value if it has been calculated or to use the old one otherwise. The iteration formula of the SOR method is

$$x^{(n+1)}_{i,\,j}=x^{(n)}_{i,\,j}-\omega\frac{r_{i,\,j}}{C_{i,\,j}}. \tag{49}$$

It can be verified theoretically for a Laplace equation that the convergence condition of Eq. (49) is to set the relaxation factor ω between 1 and 2.

The method of solving Eq. (44) is similar and therefore the procedure is simultaneously practiced.

The correspondence relation between the physical and computational domains in the present analysis is shown in Fig. 2. A solution of Laplace equations ($P=Q=0$) is obtained in Fig. 3. The calculation of viscous flows requires a grid system clustered in the vicinity of the airfoil, whereas the solution of the Laplace equations does not possess such characteristics. To obtain good clustering, one must add the sources P and Q. Following Thompson's suggestion, we assume

$$P=0,\quad Q=-\sum_1^M a_m\frac{\eta-\eta_m}{|\eta-\eta_m|}e^{-c_m|\eta-\eta_m|}, \tag{50}$$

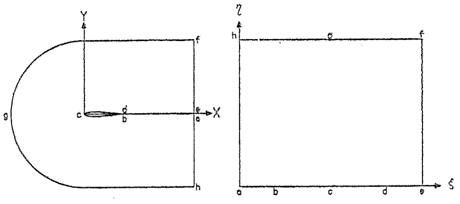

Fig. 2. Correspondence between physical and computational domains.

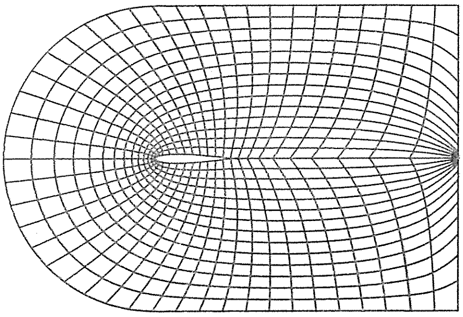

NACA 0012 47*15 [91]

Fig. 3. A solution of Laplace equations ($P=Q=0$).

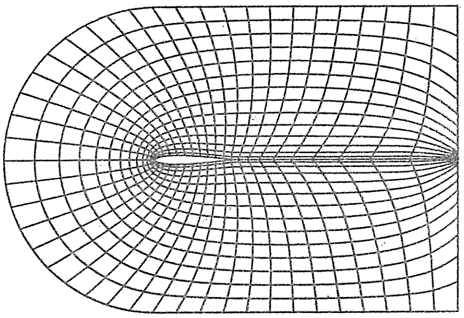

NACA 0012 47*15 [98]

Fig. 4. A solution of Poisson equations ($P=0$, Q containing one source).

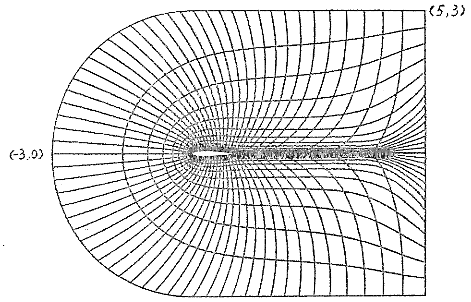

NACA 0012 65*20

Fig. 5. A solution of Poisson equations ($P=0$, Q containing five sources).

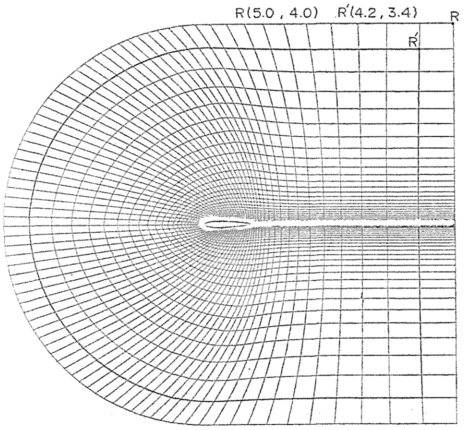

NACA 0012 83*31

Fig. 6. The grid system utilized for the present inviscid calculations.

and then solve the Poisson equations. Fig. 4 illustrates the solution obtained when applying only one source ($M=1$, $\eta_1=0$, i.e., a body source). It is shown that the clustering is obvious. Fig. 5 illustrates a result of 5 sources. It is so crowded in the vicinity of the airfoil that we can not distinguish the grids by eyes. Accompanying the clustering, unfortunately, the skewness between the cut $\overline{ab}$ ($\overline{de}$) and the lines of constant ξ becomes more serious. As a result, a difficulty occurs when we treat the boundary points on the cut with interpolation or extrapolation. Thus, we needed to find a transformation which is orthogonal on the cut. We finally achieved success for this simple airfoil contour NACA 0012, which is shown in Fig. 6 and explained in detail in the following.

Specifying the boundary points. On the airfoil surface, 51 points are distributed uniformly with an identical arc length Δs_1. On the wake cut, 16 points (other than the trailing edge point) are distributed exponentially from $x=1$ to $x=5$ with the minimum interval Δs_1. On the downstream boundary $\overline{ef}$, 31 points are distributed exponentially from $y=0$ to $y=4$ with the minimum interval 0.01 (for inviscid flow). The distribution of points on the far boundary starts from assuming a point Z which corresponds to the trailing edge point (Fig. 7). Then, 51 points are distributed uniformly on the boundary arc between Z and its symmetric point Z' with an identical arc interval Δs_2. From Z to the corner point (5, 4), 16 points (except Z) are distributed exponentially with the minimum interval Δs_2.

Parabolas. All the lines of constant ξ crossing the cut boundary are parabolas of the following form:

$$x-x_c=ay^2, \tag{51}$$

where x_c is the x-coordinate of a point on the cut and the coefficient a is determined by the coordinates of a far boundary point corresponding to that cut point. The location of point Z mentioned above is selected to let the last parabola, i.e., the one adjacent to the downstream boundary, be nearly a straight line.

Grid system in rear domain. One numerically integrates the arc length of every parabola and then chops it in proportion to the distribution of the points on the downstream boundary. The result is shown in Fig. 7.

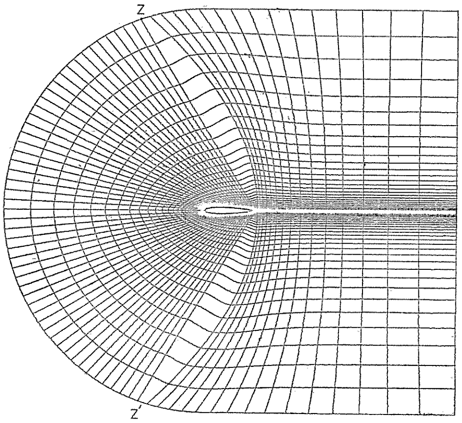

NACA 0012 83*31

Fig. 7. Rear domain is the utilized computational grid system, while the fore domain is the initial value in solving Laplace equations.

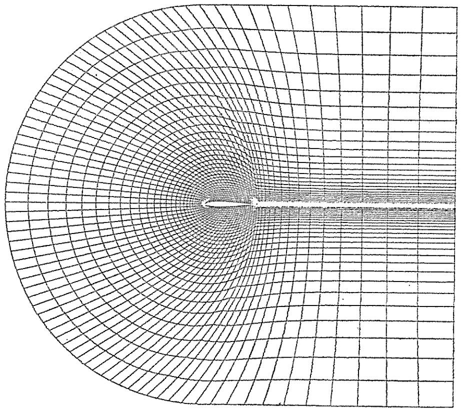

NACA 0012 83*31

Fig. 8. The fore area indicates the solution of Laplace equations.

Solving Laplace equations. The foremost parabola corresponding to the first cut point is regarded as the rear boundary of the fore domain where we solve the Laplace equations (43) and (44) with $P=Q=0$. The fore domain of Fig. 7 shows an initial attempt using linear interpolation between the airfoil surface and the far

boundary. Fig. 8 shows the result of solving the Laplace equations.
Grid system in fore domain. Numerically integrate the arc length of every line of constant ξ. Then save all the lines of constant ξ while discard all the lines of constant η. Redistribute the points along every line of constant ξ in proportion to the distribution of the points on the downstream boundary. The final result is shown in Fig. 6. The practical domain to calculate inviscid flows is slightly smaller, as indicated by the thick lines in Fig. 6, in order to obtain more accurate metric derivatives using centered differences. The coordinates of a corner point on the new downstream boundary are about (4. 2, 3. 4).

Such a transformation contains a discontinuity in the vicinity of the trailing edge, causing inaccuracy from mathematical point of view. However, the effect is not conspicuous when the trailing edge angle is rather small. In addition, the smoothness over the forward symmetric axis is not satisfied. We find, from Fig. 9, that it is better to chop the arc length in the vicinity of the leading edge into smaller intervals (not average arc length Δs_1). Although both these faults have not caused failure in later calculations, the technique of numerical grid generation still needs further progress, particularly for more complex boundaries in future.

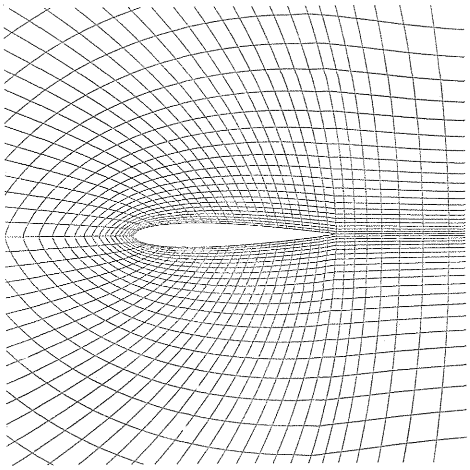

Fig. 9. Detailed grid near the airfoil.

8. Inviscid Flow

To develop a new computational technique, one always starts from simple and typical tests. We decided first to calculate an inviscid flow in order to obtain both fundamental computational experience and better initial values to calculate a viscous flow. In fact, the procedure of calculating a viscous flow is nearly identical with that of an inviscid one except that we need more complex formulas and different boundary conditions, $u=0$ and $v=0$, on an airfoil surface. It is also found that utilizing the inviscid flow solution as an initial value, the approach to the steady solution is faster. However, the calculation has to be extended up to 3-6 times the round-trip time for the disturbance to propagate over the domain; the computing time is not reduced substantially.
Initial values and boundary conditions. A calculation starts from uniform freestream variables throughout the flow field. The boundary conditions on the far boundaries are freestream ones. The values ρ, u and v on the downstream boundaries are evaluated by linear extrapolation. If three neighboring points along a curve of constant η on the physical domain are denoted by the subscripts $(i-1, j)$, (i, j) and $(i+1, j)$ and the distances are denoted as

$$\Delta l_- = \sqrt{(x_{i,\,j} - x_{i-1,\,j})^2 + (y_{i,\,j} - y_{i-1,\,j})^2},$$

$$\Delta l_+ = \sqrt{(x_{i+1,\,j} - x_{i,\,j})^2 + (y_{i+1,\,j} - y_{i,\,j})^2}, \tag{52}$$

then the condition that ρ varies linearly in this interval is expressed as

$$\frac{\rho_{i,\,j} - \rho_{i-1,\,j}}{\Delta l_-} = \frac{\rho_{i+1,\,j} - \rho_{i,\,j}}{\Delta l_+}$$

or

$$\Delta l_- \rho_{i+1,\,j} - (\Delta l_- + \Delta l_+)\rho_{i,\,j} + \Delta l_+ \rho_{i-1,\,j} = 0. \tag{53}$$

Utilizing the two known ρ values to determine $\rho_{i+1,\,j}$ (or $\rho_{i-1,\,j}$), according to the above relation, is called linear extrapolation. u and v are handled identically. Then e will be determined from Eq. (3) by assigning $p = p_\infty$. The flowfield values along the wake cut are found by merely averaging the variables of upper and lower points, i.e.,

$$U^{n+1}_{i,\,1} = (U^{n+1}_{i,\,2} + U^{n+1}_{i',2})/2, \tag{54}$$

where i' is the subscript corresponding to the reflection of i with respect to the cut.

On the airfoil surface points, ρ and $\hat{u}(\xi,\,0)$ are obtained by linear extrapolation along the lines of constant ξ as mentioned above. The impermeable condition is represented as $\hat{v}(\xi,\,0) = 0$. Then $u(x,\,y)$ and $v(x,\,y)$ are found by using Eq. (11). It is noteworthy that since the $\hat{u} = d\xi/d\tau$ is a physical quantity on $(\xi,\,\eta)$ plane, it should naturally be extrapolated on that plane. Due to the uniformity of $\Delta\eta$, the extrapolation provides

$$\hat{U}_{i,\,1} = 2\hat{U}_{i,\,2} - \hat{U}_{i,\,3}. \tag{55}$$

We implicitly solve the normal momentum equation (12) to determine p. ρ, $\hat{u}$, u_ξ and v_ξ appearing on the right-hand side of Eq. (12) are evaluated on $n+1$ level. The equation is a tridiagonal system and the first wake cut point corresponds to the boundary points on both sides of $\overline{\mathrm{bd}}$ interval on $(\xi,\,\eta)$ plane, as shown in Fig. 2. This means that the rear stagnation point is assumed at somewhere between the trailing edge and the first wake cut point. Thus, there are two values (upper and lower) at the trailing edge, although they are close together. Finally, we obtain e using Eq. (3).

From the theory of mathematics, the number of boundary conditions is determined by how many characteristic directions are pointing to the interior of a computed domain. In a supersonic flow, for example, it is four in front, three on an airfoil surface and none on downstream boundaries, etc.. However, such a basic idea is not enough for numerical calculation. We have to complement several relations to a sufficient extent. Those relations must be compatible with the original equations and boundary conditions. The complementary freestream conditions on the far and downstream boundaries are correct if the computational domain is large enough. The linear extrapolation is a first-order approximation obtained when analytically expanding from the interior to the boundary of domain. It is also correct if the spatial interval is small enough.

The $\Delta\hat{U}^n$ of the boundary points are required to construct the difference equations (28) and (29) at points adjacent to boundaries. Beam and Warming[1] derived the relations between a boundary point and two neighboring interior ones using linear extrapolation, differentiating algebraic relations and differencing differential equations. It is such a complicated procedure that we followed Steger's way where all $\Delta\hat{U}^n$ are regarded as zero. Of course, they are not truly valid unless we get to convergence to the steady solution. But a computational experiment shows that it does not prevent the process from convergence. We tested replacing $\Delta\hat{U}^n$ explicitly by $\Delta\hat{U}^{n-1}$: It turned out that the process was also convergent but did not have clearcut advantages.

Coefficient Ω of added dissipative terms. The algorithm (13) in an inviscid flow after adding dissipative terms may be written into the following form:

$$(M_1+\Omega M_2)\Delta\hat{U}^n=\Delta\tau\ (\text{sum of convection terms})+M_3\Delta\hat{U}^{n-1}-\Omega M_4 U^n, \tag{56}$$

where M_i are operators. Both $\Delta\hat{U}^n$ and $\Delta\hat{U}^{n-1}$ tend to zero when the solution converges to a steady one. Thus Eq. (56) gives a balance between sum of convection terms and added smoothing terms. On general interior points,

$$M_4U^n=O(\Delta x^4+\Delta y^4). \tag{57}$$

In particular, we will analyze the condition about Ω on the points adjacent to the airfoil, on which the smoothing terms drop to second-order differences

$$M_4U^n=O(\Delta x^2+\Delta y^2). \tag{58}$$

Each of the convection terms is an $O(1)$ quantity in an inviscid flow, so that an approximate steady solution should satisfy a condition that the sum of the convection terms is $O(\Delta x+\Delta y)$ or higher. This means that adding second-order smoothing terms is permitted, i.e., Ω may be $O(1)$. We used the central value between the stability bounds (26), i.e.,

$$\Omega=\frac{1+2\delta}{8(1+\delta)}. \tag{59}$$

Time step. We start the calculation with smaller time steps, fearing that inappropriate initial values may incur troubles, and then gradually magnify it. The calculation ceases when the elapsed time exceeds 3 times the round-trip time for a disturbance to propagate, where the propagation velocity of a disturbance is regarded as approximately 1 for the calculation of a transonic flow.

The time step is decided by choosing the Courant number N_c. It is changed as shown in the following table:

Number of iteration	0	50	100	150	350	550	750	950
Courant number N_c	1/8	1/4	1/2	1	2	4	8	16 .

The Courant number is defined as follows:

$$N_c=Max\left\{\hat{\lambda}\frac{\Delta\tau}{\Delta\xi},\ \hat{\mu}\frac{\Delta\tau}{\Delta\eta}\right\}, \tag{60}$$

where $\hat{\lambda}$ and $\hat{\mu}$ are the eigenvalues of the matrices $\hat{A}$ and $\hat{B}$, respectively. The values $\Delta\xi$ and $\Delta\eta$ may be arbitrary numbers (but not zero). We can find that they will be eliminated in Eqs. (27)-(30). For simplicity, we assume $\Delta\xi=\Delta\eta=1$.

The eigenvalues $\hat{\lambda}(\hat{A})$ and $\hat{\mu}(\hat{B})$ are derived in Apendix B:

$$|\hat{\lambda}_{max}(\hat{A})|=Max\{J[|y_\eta u-x_\eta v|+\sqrt{x_\eta{}^2+y_\eta{}^2}a]\},$$
$$|\hat{\mu}_{max}(\hat{B})|=Max\{J[|-y_\xi u+x_\xi v|+\sqrt{x_\xi{}^2+y_\xi{}^2}a]\}. \qquad (61)$$

The time interval $\Delta\tilde{\tau}$ corresponding to Courant number 1

$$\Delta\tilde{\tau}=Min\left\{\frac{\Delta\xi}{|\hat{\lambda}_{max}(\hat{A})|},\ \frac{\Delta\eta}{|\hat{\mu}_{max}(\hat{B})|}\right\}, \qquad (62)$$

is calculated at every 50 steps, because its variance is very small. Then the computational time step is set to

$$\Delta\tau=N_c\Delta\tilde{\tau}. \qquad (63)$$

Restrictions and errors. If we start from inappropriate initial values, the calculated variables often show strange behaviors, and the calculation can not be continued. To avoid this situation, it is necessary to impose artificial limits on physical quantities during unsteady modes; for example, the Mach number should not exceed M_{sup} throughout the entire flowfield (we assume $M_{sup}=2$ because we are only interested in a transonic flow). In practice, the variables must be bounded between the stagnation and M_{sup} conditions, i.e.,

$$\begin{aligned}&\rho_0\geqslant\rho\geqslant\rho_{sup},\\ &e_0\geqslant e\geqslant e_{sup},\\ &0\leqslant w\leqslant w_{sup},\\ &0\leqslant\rho w\leqslant\rho_* w_*,\end{aligned} \qquad (64)$$

where subscripts 0 and $*$ denote the stagnation ($M=0$) and critical ($M=1$) conditions, respectively.

The error at each point is evaluated by

$$\varepsilon=\frac{J}{4}\left\{\frac{|\Delta\hat{\rho}^n|}{\rho_0-\rho_{sup}}+\frac{|\Delta(\widehat{\rho u})^n|}{\rho_* w_*}+\frac{|\Delta(\widehat{\rho v})^n|}{\rho_* w_*}+\frac{|\Delta\hat{e}^n|}{e_0-e_{sup}}\right\}. \qquad (65)$$

Our program occasionally outputs the quantity $\log_{10}(\bar{\varepsilon})$ ($\bar{\varepsilon}$=root mean square error) to check whether the process is truly converging or not. If $\bar{\varepsilon}$ has exceeded 0.05, the calculation is set to automatically stop and output the subscripts i and j of all the points where $\varepsilon_{i,j}$ has exceeded $\bar{\varepsilon}$, helping us to analyze the cause.

Calculated results. We calculated four typical cases. Each case required to advance about 1000 steps corresponding to the 3 round-trip time, before converging to the steady solution:

a) $M_\infty=0.63$ and $\alpha=0°$. The solution shows an entirely subsonic flow. Fig. 10 shows the pressure distribution over the airfoil surface. We find that the pressures over the upper and lower surfaces are identical, indicating that the computational errors are negligibly small.

b) $M_\infty=0.63$ and $\alpha=2°$. Fig. 11 shows the pressure distribution. The lowest pressure of upper surface comes close to the critical one and yet the flow is subcritical. Fig. 12 shows the pressure distribution on the wake cut. We find that the pressure is flat and recovers fast to the freestream value, confirming that the selected rear boundary (3.2 chords behind the trailing edge) has been far enough.

c) $M_\infty=0.75$ and $\alpha=0°$. Fig. 13 shows the pressure distribution. The supersonic regions appear whereas there are no shock waves. The flow is supercritical. Fig. 14 indicates the converging process of the surface pressure. At each time step, the pressure distribution is regular although it has not arrived at convergence as yet.

d) $M_\infty=0.75$ and $\alpha=2°$. Fig. 15 shows the pressure distribution calculated using two different schemes, the three-level ($\theta=1$, $\delta=1/2$) and the two-level ($\theta=1$,

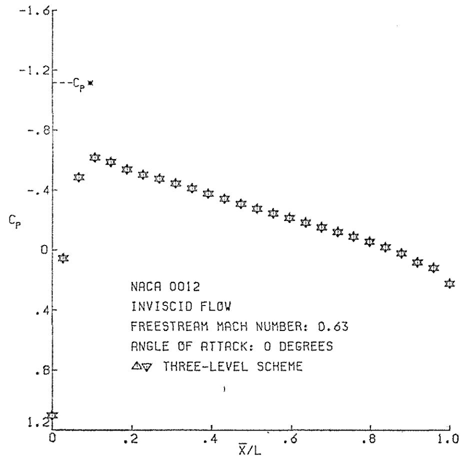

Fig. 10.

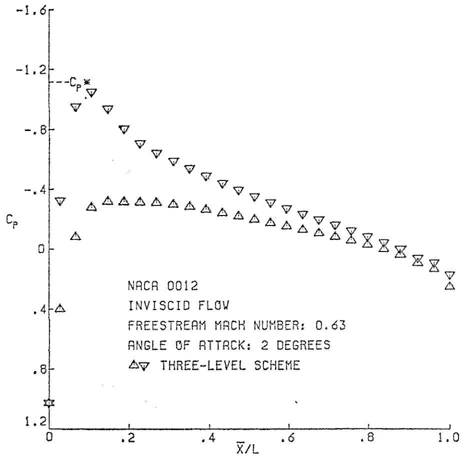

Fig. 11.

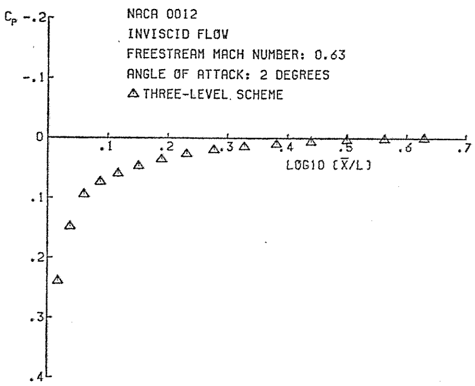

Fig. 12.

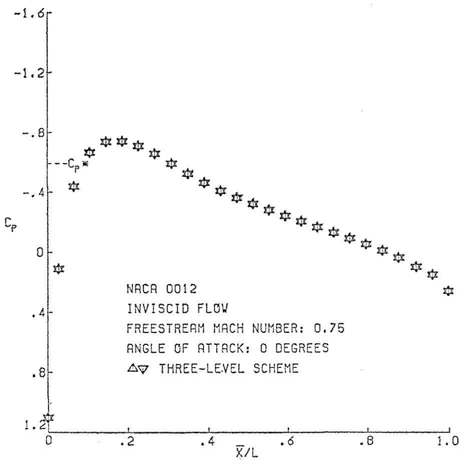

Fig. 13.

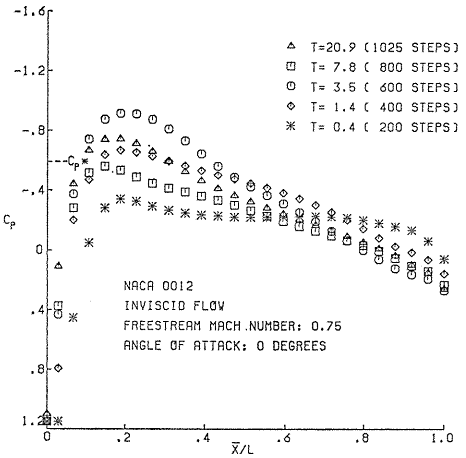

Fig. 14.

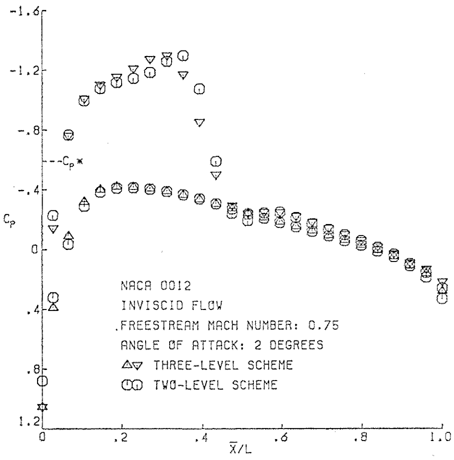

Fig. 15.

$\delta=0$) ones, respectively. A shock wave appears in the upper flowfield and therefore the flow is transonic. Both results agree sufficiently well except that the location of the shock wave calculated using the two-level scheme is slightly behind the one using the three-level scheme. Obviously, both have not generated spurious oscillations which usually appear ahead of a shock when we do not locally introduce the treatment of the upwind scheme. Fig. 16 shows the equi-Mach-number lines in the flow field.

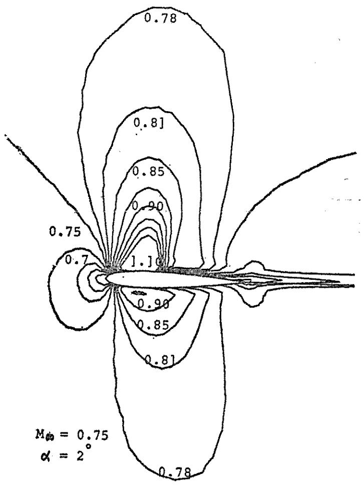

Fig. 16. The equi-Mach-number lines for $M_\infty=0.75$ and $\alpha=2°$.
(M: 0.50, 0.60, 0.65, 0.70, 0.75, 0.78, 0.81, 0.85, 0.90, 0.95, 1.00, 1.05, 1.10)

9. Viscous Flow

As mentioned previously, the procedure of calculating a viscous flow is nearly identical with that of an inviscid one. We introduce only the difference in the following.

Reclustering. To ensure a sufficient number of points within the boundary layer, reclustering of grids is necessary. This is equivalent to redistributing grid points along the lines of constant ξ. An approximate formula on the laminar boundary layer thickness of a flat plate

$$\delta_x=4.91\left(\frac{u_e x}{\nu}\right)^{-1/2}\cdot x, \tag{66}$$

is borrowed to evaluate the thickness of the conceivable boundary layer at the trailing edge ($x=1$), giving

$$\delta_1=\frac{4.91}{\sqrt{Re}}. \tag{67}$$

First, we distribute 10 points with a uniform interval $\delta_1/10$ over the downstream boundary from $y=0$ and then exponentially distribute additional 35 points starting from the minimum interval $\delta_1/10$ over the remainder. Second on each line of constant ξ, redistribute total 45 points in proportion to the distribution on the downstream boundary.

Initial values and boundary conditions. Initial values are formed by interpolating, with regard to the 35 points outside the conceivable boundary layer, using the inviscid solution and, with regard to the boundary layer, artificially constructing the other 10 points as follows:

$$\begin{aligned} u_{i,j}&=\frac{(j-1)}{10}u_{i,11} \quad (j=1, 2, \cdots, 10), \\ v_{i,j}&=\frac{(j-1)}{10}v_{i,11}, \\ p_{i,j}&=p_{i,11}, \end{aligned} \tag{68}$$

then $\rho_{i,j}$ and $e_{i,j}$ are determined from Eq. (3) and the Bernoulli formula

$$\frac{\gamma}{\gamma-1}\frac{p}{\rho}+\frac{1}{2}w^2=\frac{\gamma}{\gamma-1}p_\infty+\frac{1}{2}. \tag{69}$$

On the airfoil surface, the non-slip conditions $u=0$ and $v=0$ replace the extrapolation condition of $\hat{u}$ and the adiabatic condition

$$\frac{\partial T}{\partial n}=0,$$

or

$$-(y_\xi y_\eta+x_\xi x_\eta)T_\xi+(y_\xi^2+x_\xi^2)T_\eta=0 \tag{70}$$

replaces the extrapolation condition of ρ. Eq. (70) is implicitly solved simultaneously with Eq. (12). ρ and e are determined by Eqs. (4) and (3). We also did a test calculation not by using Eq. (70) but by extrapolating ρ. Both results agreed well.

Coefficient Ω. Eq. (56) is changed into the following form in a viscous flow:

$$\begin{aligned}(M_1+\Omega M_2)\Delta\hat{U}^n=&\Delta\tau(\text{convection terms}+\text{viscosity terms}) \\ &+M_3\Delta\hat{U}^{n-1}-\Omega M_4 U^n.\end{aligned} \tag{71}$$

Specifically we examine the situation on the points adjacent to the airfoil. The convection terms are first-order small quantities. Since we are seeking a steady solution of the N-S equations, we should make the parentheses in the right-hand side of Eq. (71) be meaningful, i.e., be second-order small quantities or higher. Considering Eq. (58), we should postulate with regard to the third term in the right-hand side

$$\Omega=\omega\cdot\Delta\tau, \tag{72}$$

where $\omega=O(1)$. We let ω be the value satisfying Eq. (59) when $\Delta\tau=(\Delta\tau)_{max}$.
Calculated results. We calculated six cases. Each one required to advance about 2000 steps corresponding to 5 round-trip time for a disturbance to propagate throughout the domain.

a) $M_\infty=0.63$, $\alpha=0°$ and $Re=10^4$. Fig. 17 describes the velocity distribution in the vicinity of the airfoil. Flow separation occurs in the neighborhood of the trailing edge and extends into the wake, where a separated area is formed. Fig. 18 shows the pressure distribution over the airfoil surface. Two different cases are compared using the three-level and two-level schemes. The latter one is based on the thin layer assumption which neglects all viscous terms in ξ-direction as well as cross derivative ones, while the right-hand side of Eq. (12) is set to zero, i.e., $\partial p/\partial n=0$. Difference between these two results is obvious on the fore part of the airfoil; because Reynolds number is too small, the thin layer assumption is not appropriate. Due to the existence of separated area, the pressure remains nearly constant in the neighborhood of the trailing edge. It is different from the corresponding inviscid flow, where the pressure continues to rise and approach the value at the rear stagnation point.

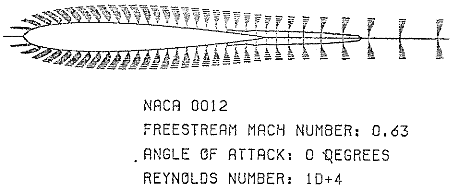

Fig. 17.

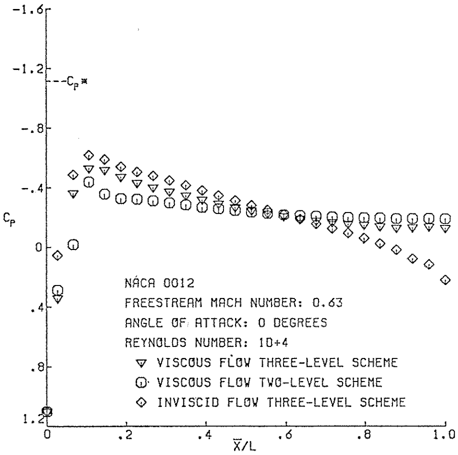

Fig. 18.

After converging to a steady state, we tried to add the terms $\hat{P}$-$\hat{Q}_\xi$ and $\hat{R}$-$\hat{S}_\eta$ and continued to calculate additional 400 steps. However, the deviation could not be recognized. This proved that the terms $\hat{P}$-$\hat{Q}_\xi$ and $\hat{R}$-$\hat{S}_\eta$ can be safely neglected in the calculation of a transonic flow.

b) $M_\infty=0.63$, $\alpha=2°$ and $Re=10^4$. Fig. 19 shows the pressure distribution. The symbol ∇ represents the upper surface and Δ the lower one. It seems strange that

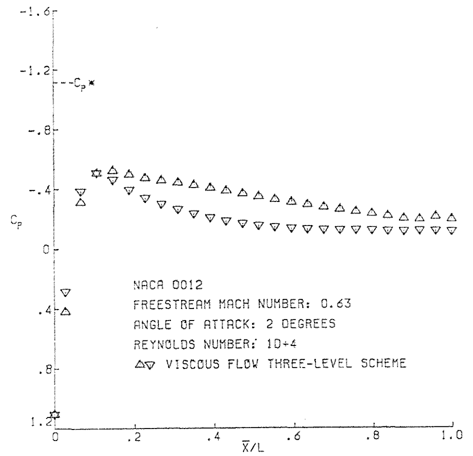

Fig. 19.

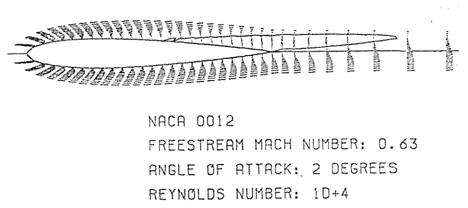

Fig. 20.

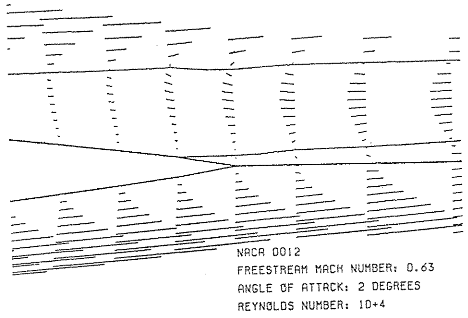

Fig. 21.

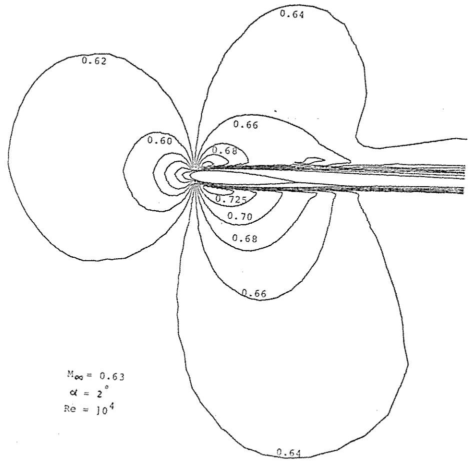

Fig. 22. The equi-Mach-number lines for $M_\infty=0.63$, $\alpha=2°$ and $Re=10^4$. (M: 0.40, 0.50, 0.55, 0.575, 0.60, 0.62, 0.64, 0.66, 0.68, 0.70, 0.725, 0.75)

the pressure over the lower surface is lower than that of the upper one, i.e., the lift is negative; maybe caused by the separation. We have not found any experimental results for comparison. Figs. 20, 21 and 22 describe the velocity distribution, indicating that the result is mathematically regular and, particularly from Fig. 22, the highest velocity of the lower half-plane is truly higher than that of the upper one. The existence of separated area is, in a sense, equivalent to the change of body shape. For such a new shape, i.e., the airfoil plus separated area, the effective angle of attack has been changed in comparison with the inviscid flow. All of the following examples have the same tendencies, which are not accidental.

c) $M_\infty=0.75$, $\alpha=2°$ and $Re=10^4$. The pressure distribution in Fig. 23 is similar to Fig. 19, showing negative lift as well. The shock wave seen in the upper inviscid flowfield disappears due to the effect of viscosity. We have changed the parameters in the following three fashions, trying to obtain a transonic flow. The results are illustrated as follows:

d) $M_\infty=0.75$, $\alpha=2°$ and $Re=10^5$. We can find in Fig. 24 that several vortices appear in the vicinity of the trailing edge, letting the calculation be incapable of converging to a steady state. The velocity distribution in the vortices is shown in

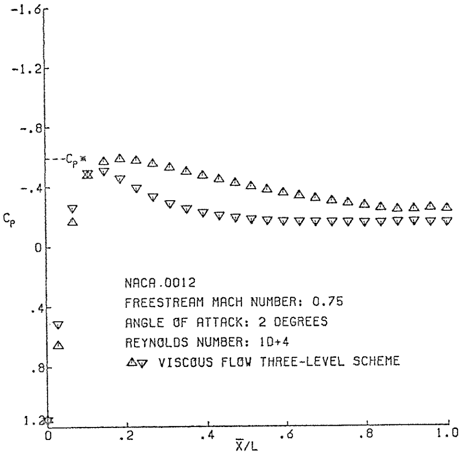

Fig. 23.

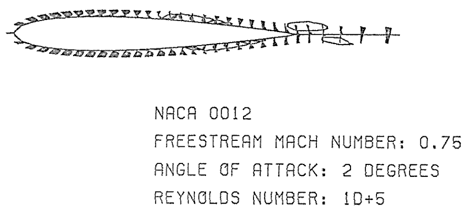

Fig. 24.

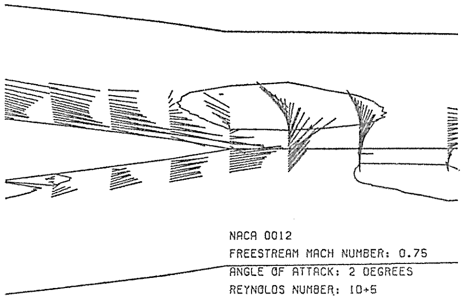

Fig. 25.

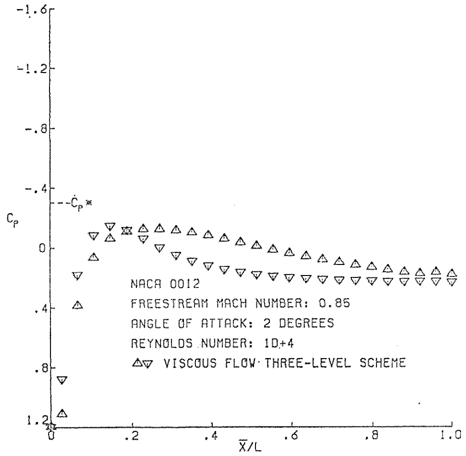

Fig. 26.

detail in Fig. 25. The result clearly indicates that it is not enough to consider only laminar flows for a high Reynolds number. The turbulence model is our next goal in the near future.

e) $M_\infty=0.85$, $\alpha=2°$ and $Re=10^4$. Fig. 26 shows that a transonic flow field has not been formed yet. A separated area expands in both forward and backward directions (see Fig. 27) and, as a result, the present computational domain appears to be insufficient. Thus, the pressure recovery on the downstream boundary is a forced rather than natural condition (see Fig. 28). To obtain a more accurate solution, the computational domain must be widened up to about 6 times the chord length according to existing experiences.

f) $M_\infty=0.75$, $\alpha=4°$ and $Re=10^4$. The pressure distribution shown in Fig. 29 is close to that in Fig. 23. In other words, the variation of α is insensitive to the pressure. From Fig. 30, we can find that the separated area expands farther in the backward direction and a new separation starts to occur below the trailing edge as well.

It may be noteworthy that the last two cases were started not from the inviscid solution but from a uniform flow outside the boundary layer as their initial conditions. Therefore, in general, the initial conditions do not need to be the

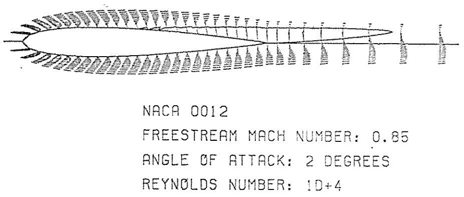

Fig. 27.

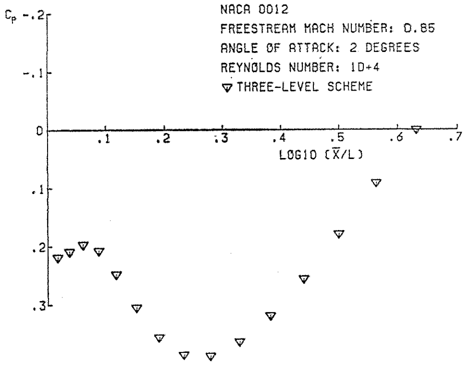

Fig. 28. The pressure distribution on the wake cut.

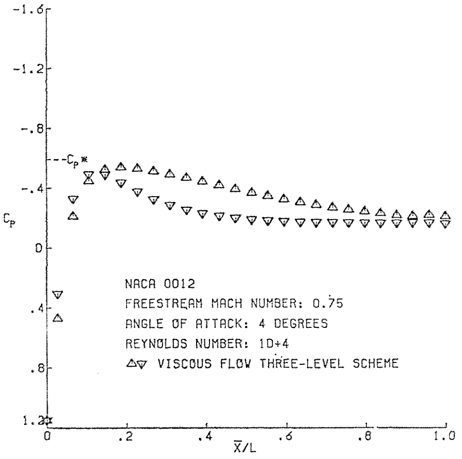

Fig. 29.

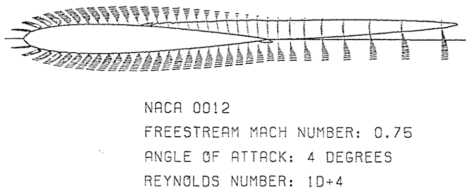

Fig. 30.

inviscid solution, in order to provide a fast and stable convergence to the steady solution. The initial conditions can be arbitrary well-behaved functions.

10. Conclusions

Numerical experiments show that an implicit, spatially factored, timewise second-order-accurate and delta-form algorithm initiated by Reference 1 is effective in solving full compressible Navier-Stokes equations. The computing cost is not very high if one vectorizes the program well enough, in other words, about 3.2×10^{-5} second VPU time and 4.7×10^{-5} second SPU time per mesh point per iterative step on a HITAC S810 super-computer. For practical applications, it is necessary to study more flexible grid generation techniques and turbulence models.

Acknowledgement

The authors would like to express their sincere appreciation to Drs. N. Hirose and K. Fujii of National Aerospace Laboratory of Japan, the Second Aerodynamics Division, for the advices on the details of computations, in particular, on the boundary conditions, smoothing terms and grids. They also are thankful to the convenience given by the Computer Centers of Nagoya University, Tokyo University and Plasma Physics Institute of Nagoya University.

Appendix A

For the algorithm of the "delta" formulation, we will utilize the first-order derivatives of the flux vectors F, G, V_1, V_2, W_1 and W_2 in Eq. (1). The Jacobian matrices A and B are

$$A=\frac{\partial F(U)}{\partial U}=$$

$$\left(\begin{array}{c:c:c:c} 0 & 1 & 0 & 0 \\ -\frac{3-\gamma}{2}u^2+\frac{\gamma-1}{2}v^2 & (3-\gamma)u & -(\gamma-1)v & \gamma-1 \\ -uv & v & u & 0 \\ -\frac{\gamma e u}{\rho}+(\gamma-1)u(u^2+v^2) & \frac{\gamma e}{\rho}-\frac{\gamma-1}{2}(3u^2+v^2) & -(\gamma-1)uv & \gamma u \end{array}\right),$$

$$B=\frac{\partial G(U)}{\partial U}=$$

$$\left(\begin{array}{c:c:c:c} 0 & 0 & 1 & 0 \\ -uv & v & u & 0 \\ -\frac{3-\gamma}{2}v^2+\frac{\gamma-1}{2}u^2 & -(\gamma-1)u & (3-\gamma)v & \gamma-1 \\ -\frac{\gamma e v}{\rho}+(\gamma-1)v(u^2+v^2) & -(\gamma-1)uv & \frac{\gamma e}{\rho}-\frac{\gamma-1}{2}(3v^2+u^2) & \gamma v \end{array}\right).$$

Before deriving other matrices, it is useful to note the following 6 sets of relations:

1) $u_\sigma=\frac{\rho u_\sigma}{\rho}=\frac{1}{\rho}[(\rho u)_\sigma-\rho_\sigma u]=\frac{1}{\rho}\left(\overline{m}_\sigma-\frac{\overline{m}}{\rho}\rho_\sigma\right)$, where σ is a coordinate direction that may be x, y, ξ or η. Thus, we have

$$\frac{\partial u_\sigma}{\partial\rho}=-\frac{\overline{m}_\sigma}{\rho^2}+\frac{2\overline{m}}{\rho^3}\rho_\sigma=-\frac{\rho_\sigma u+\rho u_\sigma}{\rho^2}+\frac{2u}{\rho^2}\rho_\sigma=-\frac{u_\sigma}{\rho}+\frac{u}{\rho^2}\rho_\sigma=-\left(\frac{u}{\rho}\right)_\sigma,$$

$$\frac{\partial u_\sigma}{\partial\overline{m}}=-\frac{\rho_\sigma}{\rho^2}=\left(\frac{1}{\rho}\right)_\sigma,\quad \frac{\partial u_\sigma}{\partial\rho_\sigma}=-\frac{u}{\rho},\quad \frac{\partial u_\sigma}{\partial\overline{m}_\sigma}=\frac{1}{\rho}.$$

2) Similarly, we have

$$\frac{\partial v_\sigma}{\partial\rho}=-\left(\frac{v}{\rho}\right)_\sigma,\quad \frac{\partial v_\sigma}{\partial\overline{n}}=\left(\frac{1}{\rho}\right)_\sigma,$$

$$\frac{\partial v_\sigma}{\partial\rho_\sigma}=-\frac{v}{\rho},\qquad \frac{\partial v_\sigma}{\partial\overline{n}_\sigma}=\frac{1}{\rho}.$$

3) $\frac{\partial(uu_\sigma)}{\partial\rho}=u_\sigma\frac{\partial u}{\partial\rho}+u\frac{\partial u_\sigma}{\partial\rho}=u_\sigma\left(-\frac{\overline{m}}{\rho^2}\right)-u\left(\frac{u}{\rho}\right)_\sigma=-\left[u_\sigma\frac{u}{\rho}+u\left(\frac{u}{\rho}\right)_\sigma\right]=-\left(\frac{u^2}{\rho}\right)_\sigma,$

$$\frac{\partial(uu_\sigma)}{\partial \overline{m}}=u_\sigma\frac{\partial u}{\partial \overline{m}}+u\frac{\partial u_\sigma}{\partial \overline{m}}=u_\sigma\frac{1}{\rho}+u\left(\frac{1}{\rho}\right)_\sigma=\left(\frac{u}{\rho}\right)_\sigma.$$

4) Likewise, we have

$$\frac{\partial(vv_\sigma)}{\partial \rho}=-\left(\frac{v^2}{\rho}\right)_\sigma,\qquad \frac{\partial(vv_\sigma)}{\partial \overline{n}}=\left(\frac{v}{\rho}\right)_\sigma.$$

5) $$\frac{\partial(vu_\sigma)}{\partial \rho}=u_\sigma\frac{\partial v}{\partial \rho}+v\frac{\partial u_\sigma}{\partial \rho}=-u_\sigma\frac{v}{\rho}-v\left(\frac{u}{\rho}\right)_\sigma=-\left[\left(\frac{uv}{\rho}\right)_\sigma+\frac{vu_\sigma-uv_\sigma}{\rho}\right],$$

$$\frac{\partial(uv_\sigma)}{\partial \rho}=-\left[\left(\frac{uv}{\rho}\right)_\sigma+\frac{uv_\sigma-vu_\sigma}{\rho}\right].$$

6) $$\frac{\partial T_\sigma}{\partial U}=\left(\frac{\partial T}{\partial U}\right)_\sigma,\qquad \frac{\partial T_\sigma}{\partial U_\sigma}=\frac{\partial\left[\sum_i \frac{\partial T}{\partial U_i}U_{i\sigma}\right]}{\partial U_\sigma}=\frac{\partial T}{\partial U},\qquad \frac{\partial T}{\partial U}=\frac{1}{\rho}\begin{pmatrix} u^2+v^2-e/\rho \\ -u \\ -v \\ 1 \end{pmatrix}.$$

Utilizing the above relations, the following 8 matrices can be easily derived:

$$QV=\frac{\partial V_1(U,\ U_x)}{\partial U_x}=\rho^{-1}\left(\begin{array}{c:c:c:c} 0 & 0 & 0 & 0 \\ \hdashline -(\lambda+2\mu)u & \lambda+2\mu & 0 & 0 \\ \hdashline -\mu v & 0 & \mu & 0 \\ \hdashline \begin{array}{l}-(\lambda+2\mu-\kappa)u^2\\ -(\mu-\kappa)v^2-\kappa e/\rho\end{array} & (\lambda+2\mu-\kappa)u & (\mu-\kappa)v & \kappa \end{array}\right),$$

$$SV=\frac{\partial V_2(U,\ U_y)}{\partial U_y}=\rho^{-1}\left(\begin{array}{c:c:c:c} 0 & 0 & 0 & 0 \\ -\lambda v & 0 & \lambda & 0 \\ -\mu u & \mu & 0 & 0 \\ -(\lambda+\mu)uv & \mu v & \lambda u & 0 \end{array}\right),$$

$$QW=\frac{\partial W_1(U,\ U_x)}{\partial U_x}=\rho^{-1}\left(\begin{array}{c:c:c:c} 0 & 0 & 0 & 0 \\ -\mu v & 0 & \mu & 0 \\ -\lambda u & \lambda & 0 & 0 \\ -(\lambda+\mu)uv & \lambda v & \mu u & 0 \end{array}\right),$$

$$SW=\frac{\partial W_2(U,\ U_y)}{\partial U_y}=\rho^{-1}\left(\begin{array}{c:c:c:c} 0 & 0 & 0 & 0 \\ \hdashline -\mu u & \mu & 0 & 0 \\ \hdashline -(\lambda+2\mu)v & 0 & \lambda+2\mu & 0 \\ \hdashline \begin{array}{l}-(\lambda+2\mu-\kappa)v^2\\ -(\mu-\kappa)u^2-\kappa e/\rho\end{array} & (\mu-\kappa)u & (\lambda+2\mu-\kappa)v & \kappa \end{array}\right),$$

$$PVX=\frac{\partial V_1(U,\ U_x)}{\partial U}=\left(\begin{array}{c|c|c|c}
0 & 0 & 0 & 0 \\
\hline
(\lambda+2\mu)_\rho u_x-(\lambda+2\mu)\left(\frac{u}{\rho}\right)_x & (\lambda+2\mu)_{\bar m}u_x+(\lambda+2\mu)\left(\frac{1}{\rho}\right)_x & (\lambda+2\mu)_{\bar n}u_x & (\lambda+2\mu)_e u_x \\
\hline
\mu_\rho v_x-\mu\left(\frac{v}{\rho}\right)_x & \mu_{\bar m}v_x & \mu_{\bar n}v_x+\mu\left(\frac{1}{\rho}\right)_x & \mu_e v_x \\
\hline
\begin{array}{l} \mu_\rho vv_x+(\lambda+2\mu)_\rho uu_x+\kappa_\rho T_x \\ -(\lambda+2\mu-\kappa)\left(\frac{u^2}{\rho}\right)_x \\ -(\mu-\kappa)\left(\frac{v^2}{\rho}\right)_x-\kappa\left(\frac{e}{\rho^2}\right)_x \end{array} & \begin{array}{l} \mu_{\bar m}vv_x+(\lambda+2\mu)_{\bar m}uu_x \\ +\kappa_{\bar m}T_x+(\lambda+2\mu-\kappa)\left(\frac{u}{\rho}\right)_x \end{array} & \begin{array}{l} \mu_{\bar n}vv_x+(\lambda+2\mu)_{\bar n}uu_x \\ +\kappa_{\bar n}T_x+(\mu-\kappa)\left(\frac{v}{\rho}\right)_x \end{array} & \begin{array}{l} \mu_e vv_x+(\lambda+2\mu)_e uu_x \\ +\kappa_e T_x+\kappa\left(\frac{1}{\rho}\right)_x \end{array}
\end{array}\right),$$

$$RVY=\frac{\partial V_2(U,\ U_y)}{\partial U}=\left(\begin{array}{c|}
0 \\
\hline
\lambda_\rho v_y-\lambda\left(\frac{v}{\rho}\right)_y \\
\hline
\mu_\rho u_y-\mu\left(\frac{u}{\rho}\right)_y \\
\hline
\begin{array}{l} \mu_\rho vu_y+\lambda_\rho uv_y \\ -\mu\left[\left(\frac{uv}{\rho}\right)_y+\frac{vu_y-uv_y}{\rho}\right] \\ -\lambda\left[\left(\frac{uv}{\rho}\right)_y+\frac{uv_y-vu_y}{\rho}\right] \end{array}
\end{array}\right.$$

$$\left.\begin{array}{c:c:c}
0 & 0 & 0 \\ \hdashline
\lambda_{\bar{m}} v_y & \lambda_{\bar{n}} v_y + \lambda\left(\dfrac{1}{\rho}\right)_y & \lambda_e v_y \\ \hdashline
\mu_{\bar{m}} u_y + \mu\left(\dfrac{1}{\rho}\right)_y & \mu_{\bar{n}} u_y & \mu_e u_y \\ \hdashline
\begin{array}{l} \mu_{\bar{m}} v u_y + \lambda_{\bar{m}} u v_y \\ + \mu v\left(\dfrac{1}{\rho}\right)_y + \lambda \dfrac{1}{\rho} v_y \end{array} & \begin{array}{l} \mu_{\bar{n}} v u_y + \lambda_{\bar{n}} u v_y \\ + \mu \dfrac{1}{\rho} u_y + \lambda u\left(\dfrac{1}{\rho}\right)_y \end{array} & \mu_e v u_y + \lambda_e u v_y
\end{array}\right),$$

$$PWX = \frac{\partial W_1(U,\ U_x)}{\partial U} = \left(\begin{array}{c:}
0 \\ \hdashline
\mu_\rho v_x - \mu\left(\dfrac{v}{\rho}\right)_x \\ \hdashline
\lambda_\rho u_x - \lambda\left(\dfrac{u}{\rho}\right)_x \\ \hdashline
\begin{array}{l} \mu_\rho u v_x + \lambda_\rho v u_x \\ -\mu\left[\left(\dfrac{uv}{\rho}\right)_x + \dfrac{u v_x - v u_x}{\rho}\right] \\ -\lambda\left[\left(\dfrac{uv}{\rho}\right)_x + \dfrac{v u_x - u v_x}{\rho}\right] \end{array}
\end{array}\right.$$

$$\left.\begin{array}{c:c:c}
0 & 0 & 0 \\ \hdashline
\mu_{\bar{m}} v_x & \mu_{\bar{n}} v_x + \mu\left(\dfrac{1}{\rho}\right)_x & \mu_e v_x \\ \hdashline
\lambda_{\bar{m}} u_x + \lambda\left(\dfrac{1}{\rho}\right)_x & \lambda_{\bar{n}} u_x & \lambda_e u_x \\ \hdashline
\begin{array}{l} \mu_{\bar{m}} u v_x + \lambda_{\bar{m}} v u_x \\ + \mu \dfrac{1}{\rho} v_x + \lambda v\left(\dfrac{1}{\rho}\right)_x \end{array} & \begin{array}{l} \mu_{\bar{n}} u v_x + \lambda_{\bar{n}} v u_x \\ + \mu u\left(\dfrac{1}{\rho}\right)_x + \lambda \dfrac{1}{\rho} u_x \end{array} & \mu_e u v_x + \lambda_e v u_x
\end{array}\right),$$

$$RWY=\frac{\partial W_2(U,\ U_y)}{\partial U}=\left(\begin{array}{c|c|c|c}
0 & 0 & 0 & 0 \\ \hline
\mu_\rho u_y-\mu\left(\frac{u}{\rho}\right)_y & \mu_{\overline{m}}u_y+\mu\left(\frac{1}{\rho}\right)_y & \mu_{\overline{n}}u_y & \mu_e u_y \\ \hline
(\lambda+2\mu)_\rho v_y-(\lambda+2\mu)\left(\frac{v}{\rho}\right)_y & (\lambda+2\mu)_{\overline{m}}v_y & (\lambda+2\mu)_{\overline{n}}v_y+(\lambda+2\mu)\left(\frac{1}{\rho}\right)_y & (\lambda+2\mu)_e v_y \\ \hline
\begin{array}{l}\mu_\rho uu_y+(\lambda+2\mu)_\rho vv_y+\kappa_\rho T_y \\ -(\lambda+2\mu-\kappa)\left(\frac{v^2}{\rho}\right)_y \\ -(\mu-\kappa)\left(\frac{u^2}{\rho}\right)_y-\kappa\left(\frac{e}{\rho^2}\right)_y\end{array} & \begin{array}{l}\mu_{\overline{m}}uu_y+(\lambda+2\mu)_{\overline{m}}vv_y \\ +\kappa_{\overline{m}}T_y+(\mu-\kappa)\left(\frac{u}{\rho}\right)_y\end{array} & \begin{array}{l}\mu_{\overline{n}}uu_y+(\lambda+2\mu)_{\overline{n}}vv_y \\ +\kappa_{\overline{n}}T_y+(\lambda+2\mu-\kappa)\left(\frac{v}{\rho}\right)_y\end{array} & \begin{array}{l}\mu_e uu_y+(\lambda+2\mu)_e vv_y \\ +\kappa_e T_y+\kappa\left(\frac{1}{\rho}\right)_y\end{array}
\end{array}\right).$$

Then, we form the following four useful matrices by combining the above 8 matrices:

$$(PVX)-(QV)_x=\left(\begin{array}{c|}
0 \\ \hline
(\lambda+2\mu)_\rho u_x+(\lambda+2\mu)_x\frac{u}{\rho} \\ \hline
\mu_\rho v_x+\mu_x\frac{v}{\rho} \\ \hline
\begin{array}{l}\mu_\rho vv_x+(\lambda+2\mu)_\rho uu_x+\kappa_\rho T_x \\ +(\lambda+2\mu-\kappa)_x\frac{u^2}{\rho} \\ +(\mu-\kappa)_x\frac{v^2}{\rho}+\kappa_x\frac{e}{\rho^2}\end{array}
\end{array}\right.$$

$$\left.\begin{array}{c:c:c}
0 & 0 & 0 \\ \hdashline
(\lambda+2\mu)_{\overline{m}}u_x-(\lambda+2\mu)_x\dfrac{1}{\rho} & (\lambda+2\mu)_{\overline{n}}u_x & (\lambda+2\mu)_e u_x \\ \hdashline
\mu_{\overline{m}}v_x & \mu_{\overline{n}}v_x-\mu_x\dfrac{1}{\rho} & \mu_e v_x \\ \hdashline
\begin{array}{l}\mu_{\overline{m}}vv_x+(\lambda+2\mu)_{\overline{m}}uu_x \\ +\kappa_{\overline{m}}T_x-(\lambda+2\mu-\kappa)_x\dfrac{u}{\rho}\end{array} & \begin{array}{l}\mu_{\overline{n}}vv_x+(\lambda+2\mu)_{\overline{n}}uu_x \\ +\kappa_{\overline{n}}T_x-(\mu-\kappa)_x\dfrac{v}{\rho}\end{array} & \begin{array}{l}\mu_e vv_x+(\lambda+2\mu)_e uu_x \\ +\kappa_e T_x-\kappa_x\dfrac{1}{\rho}\end{array}
\end{array}\right),$$

$$(RVY)-(SV)_y=\left(\begin{array}{c:}
0 \\ \hdashline
\lambda_\rho v_y+\lambda_y\dfrac{v}{\rho} \\ \hdashline
\mu_\rho u_y+\mu_y\dfrac{u}{\rho} \\ \hdashline
\begin{array}{l}\mu_\rho vu_y+\lambda_\rho uv_y \\ +(\lambda+\mu)_y\dfrac{uv}{\rho}-(\mu-\lambda)\dfrac{vu_y-uv_y}{\rho}\end{array}
\end{array}\right.$$

$$\left.\begin{array}{c:c:c}
0 & 0 & 0 \\ \hdashline
\lambda_{\overline{m}}v_y & \lambda_{\overline{n}}v_y-\lambda_y\dfrac{1}{\rho} & \lambda_e v_y \\ \hdashline
\mu_{\overline{m}}u_y-\mu_y\dfrac{1}{\rho} & \mu_{\overline{n}}u_y & \mu_e u_y \\ \hdashline
\begin{array}{l}\mu_{\overline{m}}vu_y+\lambda_{\overline{m}}uv_y \\ -\mu_y\dfrac{v}{\rho}-(\mu-\lambda)\dfrac{1}{\rho}v_y\end{array} & \begin{array}{l}\mu_{\overline{n}}vu_y+\lambda_{\overline{n}}uv_y \\ -\lambda_y\dfrac{u}{\rho}+(\mu-\lambda)\dfrac{1}{\rho}u_y\end{array} & \begin{array}{l}\mu_e vu_y+\lambda_e uv_y \\ \end{array}
\end{array}\right),$$

$$(PWX)-(QW)_x=\left(\begin{array}{c:}
0 \\ \hdashline
\mu_\rho v_x+\mu_x\dfrac{v}{\rho} \\ \hdashline
\lambda_\rho u_x+\lambda_x\dfrac{u}{\rho} \\ \hdashline
\begin{array}{l}\mu_\rho uv_x+\lambda_\rho vu_x \\ +(\lambda+\mu)_x\dfrac{uv}{\rho}+(\mu-\lambda)\dfrac{vu_x-uv_x}{\rho}\end{array}
\end{array}\right.$$

$$\left.\begin{array}{c|c|c}
0 & 0 & 0 \\ \hline
\mu_{\bar{m}}v_x & \mu_{\bar{n}}v_x-\mu_x\dfrac{1}{\rho} & \mu_e v_x \\ \hline
\lambda_{\bar{m}}u_x-\lambda_x\dfrac{1}{\rho} & \lambda_{\bar{n}}u_x & \lambda_e u_x \\ \hline
\begin{array}{l}\mu_{\bar{m}}uv_x+\lambda_{\bar{m}}vu_x \\ -\lambda_x\dfrac{v}{\rho}+(\mu-\lambda)\dfrac{1}{\rho}v_x\end{array} & \begin{array}{l}\mu_{\bar{n}}uv_x+\lambda_{\bar{n}}vu_x \\ -\mu_x\dfrac{u}{\rho}-(\mu-\lambda)\dfrac{1}{\rho}u_x\end{array} & \begin{array}{l}\mu_e uv_x+\lambda_e vu_x \\ \end{array}
\end{array}\right),$$

$$(RWY)-(SW)_y=\left(\begin{array}{c|}
0 \\ \hline
\mu_\rho u_y+\mu_y\dfrac{u}{\rho} \\ \hline
(\lambda+2\mu)_\rho v_y+(\lambda+2\mu)_y\dfrac{v}{\rho} \\ \hline
\begin{array}{l}\mu_\rho uu_y+(\lambda+2\mu)_\rho vv_y+\kappa_\rho T_y \\ +(\lambda+2\mu-\kappa)_y\dfrac{v^2}{\rho} \\ +(\mu-\kappa)_y\dfrac{u^2}{\rho}+\kappa_y\dfrac{e}{\rho^2}\end{array}
\end{array}\right.$$

$$\left.\begin{array}{c|c|c}
0 & 0 & 0 \\ \hline
\mu_{\bar{m}}u_y-\mu_y\dfrac{1}{\rho} & \mu_{\bar{n}}u_y & \mu_e u_y \\ \hline
(\lambda+2\mu)_{\bar{m}}v_y & (\lambda+2\mu)_{\bar{n}}v_y-(\lambda+2\mu)_y\dfrac{1}{\rho} & (\lambda+2\mu)_e v_y \\ \hline
\begin{array}{l}\mu_{\bar{m}}uu_y+(\lambda+2\mu)_{\bar{m}}vv_y \\ +\kappa_{\bar{m}}T_y-(\mu-\kappa)_y\dfrac{u}{\rho}\end{array} & \begin{array}{l}\mu_{\bar{n}}uu_y+(\lambda+2\mu)_{\bar{n}}vv_y \\ +\kappa_{\bar{n}}T_y-(\lambda+2\mu-\kappa)_y\dfrac{v}{\rho}\end{array} & \begin{array}{l}\mu_e uu_y+(\lambda+2\mu)_e vv_y \\ +\kappa_e T_y-\kappa_y\dfrac{1}{\rho}\end{array}
\end{array}\right).$$

Appendix B

Both $\hat{A}$ and $\hat{B}$ are the matrices of the form k_1A+k_2B. The eigenvalues are the roots of the equation $Z(\zeta)=|\zeta\cdot I-(k_1A+k_2B)|=0$. Note the matrices A and B in Appendix A and denote $\phi=k_1u+k_2v$, $\varphi=\dfrac{\gamma-1}{2}(u^2+v^2)$. Thus, we have

$$Z(\zeta)=\left|\begin{array}{c:c:c:c}
\zeta & -k_1 & -k_2 & 0 \\ \hdashline
u\psi-k_1\varphi & (\zeta-\psi)+(\gamma-2)k_1u & (\gamma-1)k_1v-k_2u & -(\gamma-1)k_1 \\ \hdashline
v\psi-k_2\varphi & (\gamma-1)k_2u-k_1v & (\zeta-\psi)+(\gamma-2)k_2v & -(\gamma-1)k_2 \\ \hdashline
\psi\left(\dfrac{\gamma e}{\rho}-2\varphi\right) & \begin{array}{c}(\gamma-1)u\psi \\ -k_1\left(\dfrac{\gamma e}{\rho}-\varphi\right)\end{array} & \begin{array}{c}(\gamma-1)v\psi \\ -k_2\left(\dfrac{\gamma e}{\rho}-\varphi\right)\end{array} & \zeta-\gamma\psi
\end{array}\right|$$

$$=\left|\begin{array}{c:c:c:c}
\zeta & -k_1 & -k_2 & 0 \\ \hdashline
-u(\zeta-\psi)-k_1\varphi & (\zeta-\psi)+(\gamma-1)k_1u & (\gamma-1)k_1v & -(\gamma-1)k_1 \\ \hdashline
-v(\zeta-\psi)-k_2\varphi & (\gamma-1)k_2u & (\zeta-\psi)+(\gamma-1)k_2v & -(\gamma-1)k_2 \\ \hdashline
\psi\left(\dfrac{\gamma e}{\rho}-2\varphi\right)-\zeta\left(\dfrac{\gamma e}{\rho}-\varphi\right) & (\gamma-1)u\psi & (\gamma-1)v\psi & \zeta-\gamma\psi
\end{array}\right|
\begin{array}{l}
\\
(\text{2nd row})-u\times(\text{1st row}) \\
(\text{3rd row})-v\times(\text{1st row}) \\
(\text{4th row})-\left(\dfrac{\gamma e}{\rho}-\varphi\right)\times(\text{1st row})
\end{array}$$

$$=\left|\begin{array}{c:c:c:c}
\zeta & -k_1 & -k_2 & 0 \\ \hdashline
-u(\zeta-\psi) & \zeta-\psi & 0 & -(\gamma-1)k_1 \\ \hdashline
-v(\zeta-\psi) & 0 & \zeta-\psi & -(\gamma-1)k_2 \\ \hdashline
\psi\left(\dfrac{\gamma e}{\rho}-2\varphi\right)-\zeta\left(\dfrac{\gamma e}{\rho}-\varphi\ \right)\ -\dfrac{\varphi}{\gamma-1}(\zeta-\gamma\psi) & u(\zeta-\psi) & v(\zeta-\psi) & \zeta-\gamma\psi
\end{array}\right|
\begin{array}{l}
(\text{1st column})-\dfrac{\varphi}{\gamma-1}\times(\text{4th column}) \\
(\text{2nd column})+u\times(\text{4th column}) \\
(\text{3rd column})+v\times(\text{4th column}) \\
\\
\end{array}$$

$$=\begin{vmatrix} \zeta-\psi & -k_1 & -k_2 & 0 \\ 0 & \zeta-\psi & 0 & -(\gamma-1)k_1 \\ 0 & 0 & \zeta-\psi & -(\gamma-1)k_2 \\ \psi\left(\frac{\gamma e}{\rho}-2\varphi\right)-\zeta\left(\frac{\gamma e}{\rho}-\varphi\right) -\frac{\varphi}{\gamma-1}(\zeta-\gamma\psi)+\frac{2}{\gamma-1}\varphi(\zeta-\psi) & u(\zeta-\psi) & v(\zeta-\psi) & \zeta-\gamma\psi \end{vmatrix} \quad \begin{array}{l}\text{(1st column)}+u\times\text{(2nd column)} \\ \quad +v\times\text{(3rd column)}\end{array}$$

$$=\begin{vmatrix} \zeta-\psi & -k_1 & -k_2 & 0 \\ 0 & \zeta-\psi & 0 & -(\gamma-1)k_1 \\ 0 & 0 & \zeta-\psi & -(\gamma-1)k_2 \\ \psi\left(\frac{\gamma e}{\rho}-2\varphi\right)-\zeta\left(\frac{\gamma e}{\rho}-\varphi\right) -\frac{\varphi}{\gamma-1}(\zeta-\gamma\psi)+\frac{2}{\gamma-1}\varphi(\zeta-\psi) & 0 & 0 & \zeta-\psi \end{vmatrix}. \quad \begin{array}{l}\text{(4th row)}-u\times\text{(2nd row)} \\ \quad -v\times\text{(3rd row)}\end{array}$$

Due to

$$\psi\left(\frac{\gamma e}{\rho}-2\varphi\right)-\zeta\left(\frac{\gamma e}{\rho}-\varphi\right)-\frac{\varphi}{\gamma-1}(\zeta-\gamma\psi)+\frac{2}{\gamma-1}\varphi(\zeta-\psi)$$

$$=-(\zeta-\psi)\left(\frac{\gamma e}{\rho}-\frac{\gamma}{\gamma-1}\varphi\right)$$

and

$$\frac{\gamma e}{\rho}-\frac{\gamma}{\gamma-1}\varphi=\frac{\gamma}{\rho}\left[e-\frac{1}{2}\rho(u^2+v^2)\right]=\frac{\gamma p}{(\gamma-1)\rho}=\frac{1}{\gamma-1}a^2$$

(a=sonic velocity),

the characteristic equation is written as

$$Z(\zeta)=\begin{vmatrix}\zeta-\varphi & -k_1 & -k_2 & 0\\ 0 & \zeta-\varphi & 0 & -(\gamma-1)k_1\\ 0 & 0 & \zeta-\varphi & -(\gamma-1)k_2\\ -(\zeta-\varphi)\frac{a^2}{\gamma-1} & 0 & 0 & \zeta-\varphi\end{vmatrix}$$

$$=(\zeta-\varphi)\begin{vmatrix}\zeta-\varphi & 0 & -(\gamma-1)k_1\\ 0 & \zeta-\varphi & -(\gamma-1)k_2\\ 0 & 0 & \zeta-\varphi\end{vmatrix}$$

$$+(\zeta-\varphi)\frac{a^2}{\gamma-1}\begin{vmatrix}-k_1 & -k_2 & 0\\ \zeta-\varphi & 0 & -(\gamma-1)k_1\\ 0 & \zeta-\varphi & -(\gamma-1)k_2\end{vmatrix}$$

$$=(\zeta-\varphi)^4-(\zeta-\varphi)^2(k_1^2+k_2^2)a^2=(\zeta-\varphi)^2[(\zeta-\varphi)^2-(k_1^2+k_2^2)a^2]=0,$$

the four eigenvalues of which are k_1u+k_2v, k_1u+k_2v, $k_1u+k_2v+\sqrt{k_1{}^2+k_2{}^2}\,a$ and $k_1u+k_2v-\sqrt{k_1{}^2+k_2{}^2}\,a$.

Substituting various values into k_1 and k_2, we obtain the following table:

matrix	k_1	k_2	eigenvalues
A	1	0	$u,\ u,\ u+a,\ u-a$
B	0	1	$v,\ v,\ v+a,\ v-a$
$\hat{A}$	Jy_η	$-Jx_\eta$	$J(y_\eta u-x_\eta v),\ J(y_\eta u-x_\eta v),\ J[(y_\eta u-x_\eta v)+\sqrt{x_\eta{}^2+y_\eta{}^2}\,a],$ $J[(y_\eta u-x_\eta v)-\sqrt{x_\eta{}^2+y_\eta{}^2}\,a]$
$\hat{B}$	$-Jy_\xi$	Jx_ξ	$J(-y_\xi u+x_\xi v),\ J(-y_\xi u+x_\xi v),\ J[(-y_\xi u+x_\xi v)+\sqrt{x_\xi{}^2+y_\xi{}^2}\,a],$ $J[(-y_\xi u+x_\xi v)-\sqrt{x_\xi{}^2+y_\xi{}^2}\,a]$

References

1) R. M. Beam and R. F. Warming; An Implicit Factored Scheme for the Compressible Navier-Stokes Equations, AIAA Journal, Vol. 16, pp. 393-402, 1978.

2) J. L. Steger; Implicit Finite-Difference Simulation of Flow about Arbitrary Two-Dimensional Geometries, AIAA Journal, Vol. 16, pp. 679-686, 1978.

3) N. Satofuka; Modified Differential Quadrature Method for Numerical Solution of Multi-Dimensional Flow Problems, Proceedings of International Symposium on Applied Mathematics and Information Sciences, Kyoto University, March 1982.

4) R. F. Warming and R. M. Beam; Upwind Second-Order Difference Schemes and Applications in Aerodynamic Flows, AIAA Journal, Vol. 14, pp. 1241-1249, 1976.

5) C. M. Hung and R. W. MacCormack; Numerical solutions of Supersonic and Hypersonic Laminar Compression Corner Flows, AIAA Journal, Vol. 14, pp. 475-481, 1976.

6) Y. Y. Wang and T. Fujiwara; The Numerical Analysis of Transonic Flow around a Circular Airfoil Using Hybrid Difference Scheme, Memoirs of the Faculty of Engineering, Nagoya University, Vol. 36, No. 1, pp. 68-78, 1984.

7) R. M. Beam and R. F. Warming; An Implicit Finite-Difference Algorithm for Hyperbolic Systems in Conservation-Law Form, Journal of Computational Physics, Vol. 22, pp. 87-110, 1976.

8) American Institute of Physics Handbook, Second Edition, p. 2-222 and 2-226, McGraw-Hill Book Company, Inc., 1963.

9) J. L. Steger; On Application of Body Conforming Curvilinear Grids for Finite Difference Solution of External Flow, "Numerical Grid Generation", pp. 295-316, NORTH-HOLLAND, 1982.

10) W. J. Gordon and L. C. Thiel; Transfinite Mappings and Their Application to Grid Generation, "Numerical Grid Generation", pp. 171-192, NORTH-HOLLAND, 1982.

11) D. C. Ives; Conformal Grid Generation, "Numerical Grid Generation", pp. 107-136, NORTH-HOLLAND, 1982.

12) J. F. Thompson; General Curvilinear Coordinate Systems, "Numerical Grid Generation", pp. 1-30, NORTH-HOLLAND, 1982.

13) J. F. Thompson; Elliptic Grid Generation, "Numerical Grid Generation", pp. 79-105, NORTH-HOLLAND, 1982.

14) F. C. Thames, J. F. Thompson, C. W. Mastin and R. L. Walker; Numerical Solutions for Viscous and Potential Flow about Arbitrary Two-Dimensional Bodies Using Body-Fitted Coordinate Systems, Journal of Computational Physics, Vol. 24, pp. 245-273, 1977.